Nuclear Engineering and Design 379 (2021) 111188

Contents lists available at ScienceDirect

Nuclear Engineering and Design

journal homepage: www.elsevier.com/locate/nucengdes

Literature survey of droplet entrainment from water pools

M. Ouallal [a,*], S. Leyer [a], S. Gupta [b]

[a] Faculty of Science, Technology and Communication, University of Luxembourg, Campus Kirchberg, Luxembourg L-1359, Luxembourg
[b] Becker Technologies GmbH, Rahmann Straße 11, 65760 Eschborn, Germany

ARTICLE INFO

Keywords:
Pool scrubbing
Entrainment
Superficial gas velocity
Droplets

ABSTRACT

The present paper aims to study the phenomena of droplet entrainment from water pool. This phenomena could be either a consequence of boiling or depressurization. In a bubble column, droplets are released at the surface of the pool by bursting (in bubbly flow regime) or by detachment (in churn turbulent flow regime) depending of the hydrodynamics inside the pool. Eventually, these droplets are entrained by the streaming gas (superficial gas velocity) or settling down due to gravity.

Many experimental studies have been conducted, and several numerical simulations were performed to a better understanding of the phenomena of entrainment. Numerical simulation are a good tool to simulate an experiment due to limitations of data. To that end, CFD showed to be a good candidate to perform such a simulation, yet demand high computational performance and are time consuming. However, Lumped Parameter codes (LP) are widely used due to their simplicity and fast running, nevertheless, only provides qualitative and quantitative data. This paper gives a detailed review on the phenomena of entrainment covering experimental, analytical work. Relevant details on pool scrubbing are also provided for completeness purposes.

1. Introduction

The entrainment of liquid phase by a gas phase is found in a numerous industrial process, where mass and heat transfer intervene. During the interaction liquid-gas, the formation of the droplets is a common phenomenon. Taking their size into account, and the exchange with the gas phase, they can be entrained by this latter to a specific height above the water surface. The gas phase is characterized by the superficial gas velocity.

The superficial gas velocity is calculate from the volume flow rate of the gas coming from the pool surface of a certain cross section area. Therefore, for different superficial gas velocities comes different flow regimes in the water pool. At low superficial gas velocities, the regime is attributed to a bubbly flow regime, where bubble are defined in shapes and size (Shah et al., 1982). At high superficial gas velocities, where the irregular shapeless bubble are formed, the regime is attributed to churn turbulent flow. As a function of the flow regimes, the droplet generation mechanism differs, from bubble burst to detachment from liquid ligaments due to momentum exchange gas–liquid. The present study concerns the release of these droplets, or so called droplet entrainment from water pool that cover the mentioned flow regimes.

The phenomenon of entrainment is found in industrial processes as in natural phenomena, from geophysics (release of salt from the surface of the sea), water treatment (desalination) to nuclear applications (release of aerosol from water pool).

In natural phenomena, the entrainment is responsible of mass transfer at the surface of the sea. Sea spray, which is the amount of droplets generated either from bubble burst or roll wave or by splashing containing salts and bacteria from the sea surface (Blanchard, 1989) (Spiel, 1998a, 1998b) are entrained by the wind and could be problematic for human health as it could affect the climate. The released aerosol might form large clouds that could affect the air quality as well as reflecting the sun light. The weather in coastal region is mainly determined by quantifying the amount of airborne aerosols.

In the sector of water treatment, in order to separate solid from liquid phase, desalination plants use evaporator. The process is to entrain droplet by injecting steam. As the bubbles rise to reach the surface, they burst to generate small droplets that are partly entrained in the distillate.

In horizontal and vertical separators in gathering centres, to separate phases (gas, oil and liquid), a mixture of gas–water-oil or gas-oil is feed into a static vessel. The inflow causes agitation of the interface by entraining gas into the mixture of oil-liquid in form of bubbles. This latter rise on the surface and burst producing droplets. Therefore, for phase separation, gas is exhausted by a vent at the top of the vessel,

* Corresponding author.
E-mail addresses: mohammed.ouallal.002@student.uni.lu (M. Ouallal), stephan.leyer@uni.lu (S. Leyer), gupta@becker-technologies.com (S. Gupta).

https://doi.org/10.1016/j.nucengdes.2021.111188
Received 9 November 2020; Received in revised form 3 March 2021; Accepted 7 March 2021
Available online 3 April 2021

carrying liquid droplet with it. One of the principle of separation is coalescence. Coalescing is related to the agitation process. During coalescence, water droplets come together to form larger drops. In vane type mist eliminators, droplets are removed from the vapour stream through inertial impaction. The wet gas is forced to change direction causing mists droplets to strike the vanes and coalesce with other droplets eventually falling. However some of the droplets escape without coalescing. Therefore, the amount of droplet needs to be quantified in order to measure the purity of the gas (Viles, 1993) (Kharoua et al., 2013) (Wurster et al., 2015).

In nuclear engineering, the Steam Generator Tube Rupture (SGTR) events often occurs during PWR operation. The steam generator tube might experience degradations that cause leakage or rupture (Dehbi et al., 2016). Water from the primary circuit passes in the secondary circuit by large quantities transporting fission products along. The steam generator is rapidly filled with water, and droplets might be released due to boiling from the pool to the environment through vents. Therefore, the quantification of these droplet is necessary from the design point of view (Berzal et al., 1995) (Bagul et al., 2018b) (Qiu et al., 2015).

In BWR severe accident, after the core damage, a mixture of steam/non-condensable gases and FPs is transported via pipe into large water pool. Some of the FP will become trapped in the water pool and some of them will be re-entrained by the streaming gas due to the continuous heat release or boiling. The consequence of the gas release into the containment building atmosphere, also caused by release of H_2 and CO from MCCI, could jeopardize the containment integrity. Therefore, the building is depressurized using vents placed at a certain height above the water pool. The depressurization may induce boiling, and the rate of depressurization defines the hydrodynamic of the pool. High depressurization rates cause large agitation in water pool by producing large bubble (Kudo et al., 1994), whereas low depressurization rates engender small bubbles at the water surface (Freitag and Schmidt, 2017). In either case, the release of droplet from water pool as a function of the flow regime is inevitable. These droplets re-entrain contaminants (such as aerosol) and might contribute to their release to the environment.

The assessment of the entrainment phenomena is conducted by numerical simulation. CFD and LP codes are used for this purpose. CFD simulations require computational resources to simulate small droplets in the micron range and provide as well results on the characteristics of the droplets including their size and velocity distributions at different height above the water pool, in addition to their concentration. Nonetheless, this amount of information are time consuming to acquire. Whilst LP codes are characterized by short time execution and providing results in a couple of minutes due to their empirical aspect. LP code are popular in simulating severe accidents scenarios in power plants.

In the open literature, experiments conducted on entrainment in large pool and large vessel are limited to low superficial gas velocities (bubbly flow regime), and experiments conducted in small pools used high superficial gas velocities. In addition, entrainment models that could be found in literature have limited range of applicability in terms of the flow regime (high superficial gas velocity) and/or geometry.

A prior understanding of the dynamics of the bubble is imperative, such as the effect of thermal hydraulics, physical properties of the liquid, bubble behaviour at the surface of the pool before and after the burst for simple cases such as the study of a single bubble to quantify the entrainment. Then, the information on the single bubble could be translated to bubble swarm by analysing the behaviour of the bubbles at the water surface under low and high gas flow rates. The objective of this review is to provide a state of the art of the phenomenon of entrainment including relevant experiments conducted in different facilities to simulate different accident scenarios in NNP and mechanistic models. Additionally, to demonstrate the main shortcoming of such a models.

This review will be organized as follows: The first part deals with a brief description of pool scrubbing phenomena, and existing computer codes in the literature to analyse it. The second part includes the phenomena of Entrainment and the previous theoretical work. The third part is dedicated to Entrainment experimental work, and the last part summarizes and discusses the opening issue.

2. Phenomenology of pool scrubbing and entrainment

2.1. Pool scrubbing

BWR and PWR severe accident scenarios involve the transportation of radioactive aerosols through large water pools in which particles can be retained. This phenomenon, known as pool scrubbing, has the potential to reduce the source term. The action of the gas-aerosols mixture passing through the water pool from a submerged pipe to the surface strongly depends on the inlet aerosol-gas mixture when it enters the pool through several vent types (downcomer, horizontal vents, quencher…). Condensable and non-condensable gases exhibit different behaviour when passing through the vent into a water pool. Gases, such as steam, may condense inside the vent pipe (in the case of low gas flux) in subcooled water pool.

The size of the bubble formed at the inlet depends on the injection type and the gas flow rate. For a downcomer and low gas flow rates, a large bubble (a globule) is formed, detaches and breaks up into smaller bubbles of different sizes, which eventually rise to the pool surface. The time for the swarm of bubbles to rise depends on the gas flux, the gas composition and the vent submergence. The intensity of coalescence and the breakup of the bubbles depend on the gas flow rates. The bubble hydrodynamics plays a key role in the triggering of the physical phenomena for aerosol retention. For instance, assuming a single bubble is rising in water pool, the bubble shape depends on its size. The shear stress and the liquid density cause the bubbles to move in a top-to-bottom rotation. This bubble rotation causes centrifugal forces, which favour the retention of large aerosol particles from the bubble into the water pool (Owczarski and Burk, 1991).

Therefore, the hydrodynamics of the pool requires the description of shape and motion of the gas bubbles as a function of its diameter, and the Reynolds number as given in Table 1 (Özdemir, 2005).

The thermal hydraulics of the pool/gas affects particle retention. The heat and mass transfer to and from the gas depends on the gas composition. The migration of particles from the gas bubbles into the water pool is a consequence of the driving forces. Pycnophoresis, which is driven by the density gradient, arises from respective temperature (thermophoresis) and pressure gradients (barodiffuion) (Brenner, 2011). Diffusiophoresis is driven by the macroscopic concentration gradient of the molecular solute.

The assessment of hydrodynamics and thermal-hydraulics of the pool from the injection point, in addition to experiments, is made by means of numerical simulation. Such phenomena need relevant computational resources to be conducted using CFD codes. It is essential to simulate the complex physical phenomena under suitable assumption for better understanding. Lumped parameter codes show to be better candidate.

Table 1
Shape and motion of gas bubbles as a function of d_b and Re in a stagnant large water pool.

Diameter range	Reynolds number range	Bubble behaviour
$d_b < 0.8$ mm	$Re < 70$	Spherical bubbles in rectilinear motion
$0.8 < d_b < 1.24$ mm	$70 < Re < 400$	Spherical bubbles in rectilinear motion
$1.24 < d_b < 1.54$ mm	$400 < Re < 500$	Oblate spheroid bubbles in rectilinear motion
$1.54 < d_b < 4.8$ mm	$500 < Re < 1100$	Oblate spheroid bubbles in helicoidal motion
$4.8 < d_b < 7$ mm	$1100 < Re < 1600$	Irregular oblate spheroid, almost rectilinear motion
$7 < d_b < 17.6$ mm	$1600 < Re < 5000$	Oblate spheroid to spherical cap, almost rectilinear motion
$d_b > 17.6$ mm	$Re > 5000$	Spherical caps, rectilinear motion

There are several lumped parameter codes that feature models which emphasize bubble generation under the above-mentioned injection scenarios. In essence, these codes are developed to calculate the decontamination factor of flows which contain aerosols under different flow regimes (from the bubble flow regime to the turbulent flow regime). Some of the pool scrubbing codes are mentioned below.

SPARC-90 (Suppression Pool Aerosol Removal Code) developed by the Pacific Northwest Laboratory (Owczarski and Burk, 1991), in order to calculate the decontamination factor for flow containing aerosols in the suppression pools of BWR:

SPARC-B/98 developed by GRS Germany (Schmitz, 2000).

BUSCA (BUbble SCrubbing Algorithm) results from the collaboration between AEA United Kingdom Institutions, GRS in Germany, UPM Spain and PSI of Switzerland (Ramsdale, 1995) as a code designed to determine decontamination factors in the pool of water covering the melted core in severe accident conditions;

BUSCA-PSI is the result of changes made by PSI Switzerland (Tables 2 and 3) (Dehbi and Guentay, 1994).

SUPRA (SUppression Pool Retention Analysis) was developed by EPRI (Electric Power Research Institute) (Wassel et al., 1985) to calculate the retention of aerosol particles and gaseous fission products passing through the water in the pool;

ECART (Enel Code for Analysis of Radionuclide Transport) was developed by ENEL research (Parozzi and Paci, 2006) (now know-how in RSE) in order to estimate the realistic release of toxic or radioactive substances resulting from a severe accident.

ART developed by the Japan Atomic Energy Research institute (Tables 2 and 3) (Kajimoto et al., 1988).

The abovementioned code give results on: the size and the shape of the gas–water interface until the formation of the globule, the mass, momentum and energy at that interface, bubble residence and rising time, and natural physical processes for particle retention.

Four zones are distinguished from the injection to the water surface as a function of the inlet gas flux. The bubble dynamics changes with gas flux and injection type (from discrete bubble of the same size to a distribution of bubble sizes). (Figure 29 in (Berzal et al., 1995)).

After retention of the particle by means of natural physical processes, the bubble swarm might also contain particles while reaching the surface of the pool.

2.2. Entrainment

As the gas continues to discharge into the pool, the same physical processes perform the transportation function from the pool inside the bubble as shown in Fig. 1. In addition to the retention mechanisms, the mixing in the sump causes the agitation of retained particles. This agitation is caused by the rising of the bubble swarm toward the surface, which also acts as a pump (Owczarski and Burk, 1991).

The particles (soluble or solid) are released from the pool to the containment atmosphere in the form of droplets by droplet generation mechanisms.

As for droplet generation, there are several mechanisms which depend on the gas velocity. In the bubbly flow regime, the bubbles rise as a swarm, reach the surface forming a spherical cap. The time for this cap to burst and generate droplets depends on the bubble size and physical properties of the fluid (viscosity, density, surface tension) and the thermal–hydraulic of the pool and gas atmosphere above the water-surface. Poulain (Poulain et al., 2018) investigated this effect of bubble ageing in detail. Zhang et al. (2012) demonstrated that the bubble has a critical size where no jet drops are produced which means less entrainment. As an example, high viscous fluids exhibit clear effect on entrainment as the number of droplets produced by bubble-burst decreases drastically. Ramirez (de Santiago and Marvillet, 1991), (Lhuissier and Villermaux, 2012) and (Poulain et al., 2018) investigated this effect and more in great detail.

The aerosols are re-entrained not only by the discharged gas, but also

Table 2
Removal mechanism in various codes.

Code zone	ART	BUSCA	BUSCA-PSI	SUPRA	SPARC	SPARC-B/98	ECART
Inlet	Not considered	Not considered	Jet impaction	Not considered	Not considered	impaction and interception by droplets; molecular and turbulent diffusion to droplets; vapour condensation,/ diffusiophoresis, thermophoresis and Brownian diffusion to the jet wall	Sedimentation Centrifugal impaction; Brownian diffusion; Condensation
Primary bubbles	Not considered	inertial impaction sedimentation Brownian diffusion	Sedimentation Brownian diffusion Centrifugal deposition: Diffusiophoresis;	Inertial impaction; Centrifugal deposition;	Vapour condensation Sedimentation Inertial impaction Brownian diffusion; Centrifugal deposition;	Vapour condensation/ Diffusiophoresis Sedimentation Inertial impaction Brownian diffusion Thermophoresis Centrifugal deposition	Sedimentation Centrifugal impaction; Brownian diffusion;
Bubble rising	Sedimentati-on Centrifugal deposition	Centrifugal deposition diffusiophoresis thermophoresis breakup	Sedimentation Brownian diffusion; Centrifugal deposition; Diffusiophoresis Breakup	Sedimentation Brownian diffusion; Centrifugal deposition; Diffusiophoresis Thermophoresis	Sedimentation; Brownian diffusion; Centrifugal deposition; Diffusiophoresis; Breakup;	Sedimentation; Brownian diffusion; Centrifugal deposition; Diffusiophoresis	Sedimentation Centrifugal impaction Brownian diffusion

Table 3
Thermal hydraulics of Pool Scrubbing codes.

Codes	ART	BUSCA	BUSCA-PSI	SUPRA	SPARC	SPARC-B/98	ECART
Thermohydraulics							
Models for the jet region	Not considered	Not considered		Steam cone model	Not considered	For quencher or single orifice injection, an immersed jet is modelled for high injection velocity.	Not considered
Primary bubble volume	user specifies	1.user specifies; 2.Ramakrishnan et al's theoretical model;3. EPRI's horizontal and vertical vent correlations; 4.SPARC'S horizontal vent, downcomer and quencher correlations	1.user specifies; 2.Ramakrishnan et al's theoretical model;3. EPRI's horizontal and vertical vent correlations; 4.SPARC'S horizontal vent, downcomer and quencher correlations	Surface tension and buoyancy balance. User define. Ramakrishnan et al model. Reynolds number at orifice correlation.	SPARC'S horizontal vent, downcomer and quencher correlation	SPARC'S horizontal vent, downcomer and quencher correlation;	EPRI horizontal vent EPRI vertical vent
Rising bubble size	The same as primary bubble	lognormal size distribution, average diameter is 0.716m	lognormal size distribution, average diameter is 0.716m	Leibson et al's Correlation	Single diameter which depends on the steam fraction in injected gas	Superposition of two lognormal size distributions	Equivalent sphere
Bubble shape	sphere	1.sphere; 2.oblate ellipsoid; 3. spherical ca	1.sphere; 2.oblate ellipsoid; 3. spherical ca	Sphere Oblate spheroid Spherical cap	Oblate ellipsoid	Oblate ellipsoid	Oblate ellipsoid
Velocity of rising bubble	1.user specifies 2.calculated by THALES	1.correlation of the Five Wallis Regimes 2.correlation for spherical, oblate ellipsoid, spherical cap bubble shape respectively	1.correlation of the Five Wallis Regimes 2.correlation for spherical, oblate ellipsoid, spherical cap bubble shape respectively	Haberman and Morton data. Peebles and Garber, Haberman and Morton, Wallis.	Two correlations based on Haberman et al's data	SPARC-90	
Swarm rise velocity	1.user specifies 2.calculated by THALES	1.GEC cluster model;2. Colder cluster model; 3. Sjoen plume model	1.GEC cluster model; 2. Colder cluster model; 3. Sjoen plume model	Not available	Correlation based on data from Paul et al and GE company	New correlations that considers the influence of finite water pool size	SPARC's
Temperature of bubble interface	Not available	Assume bubble interface is at pool temperature	Assume bubble interface is at pool temperature	Different from pool and bubble gas temperature, calculated additionally	Different from pool and bubble gas temperature, calculated additionally	Different from pool and bubble gas temperature, calculated additionally	User defines

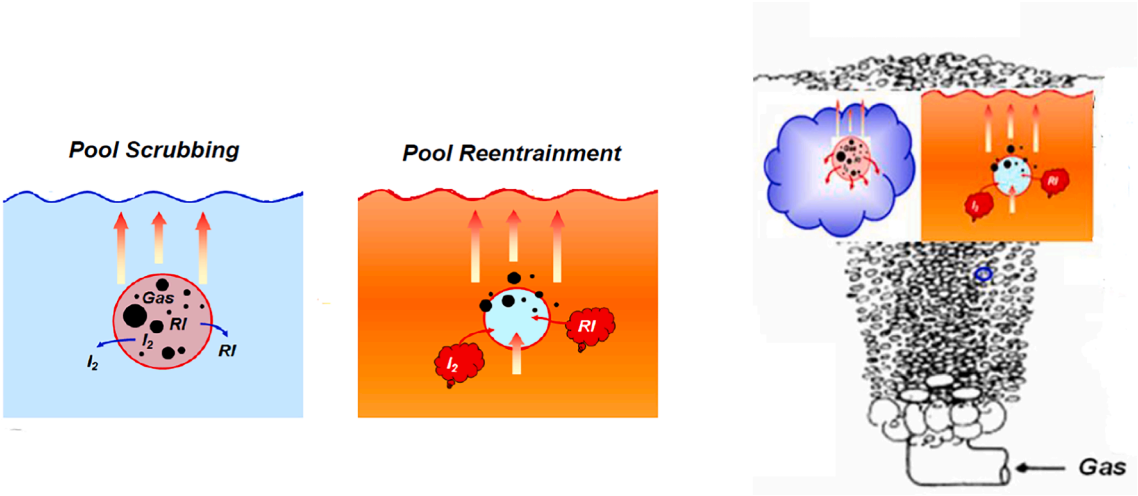

Fig. 1. Pool scrubbing and re-entrainment phenomena (Gupta and Herranz, 2017).

by depressurization of the containment that may occur either due to venting operations or leakages. The decrease in pressure may also induce boiling. The resulting flow-regimes caused by depressurization-induced boiling may range from bubbly to churn turbulent. Thus, the droplet generation mechanism is a strong function of the pressure reduction rate and the vent position. This phenomenon was investigated in the past, as reported in (Freitag and Schmidt, 2017), (Kudo et al., 1994), (Cosandey, 1999). Fig. 2 shows different mechanisms of droplet generation.

The mechanisms that could be manifested in a containment water pool are bubble burst (low gas velocity), shear of ligament by streaming gas (high gas velocity) and liquid impingement caused by splashing waves against containment walls or each other. Droplet generation by roll waves (cocurrent two-phase flow) and wave undercut (counter

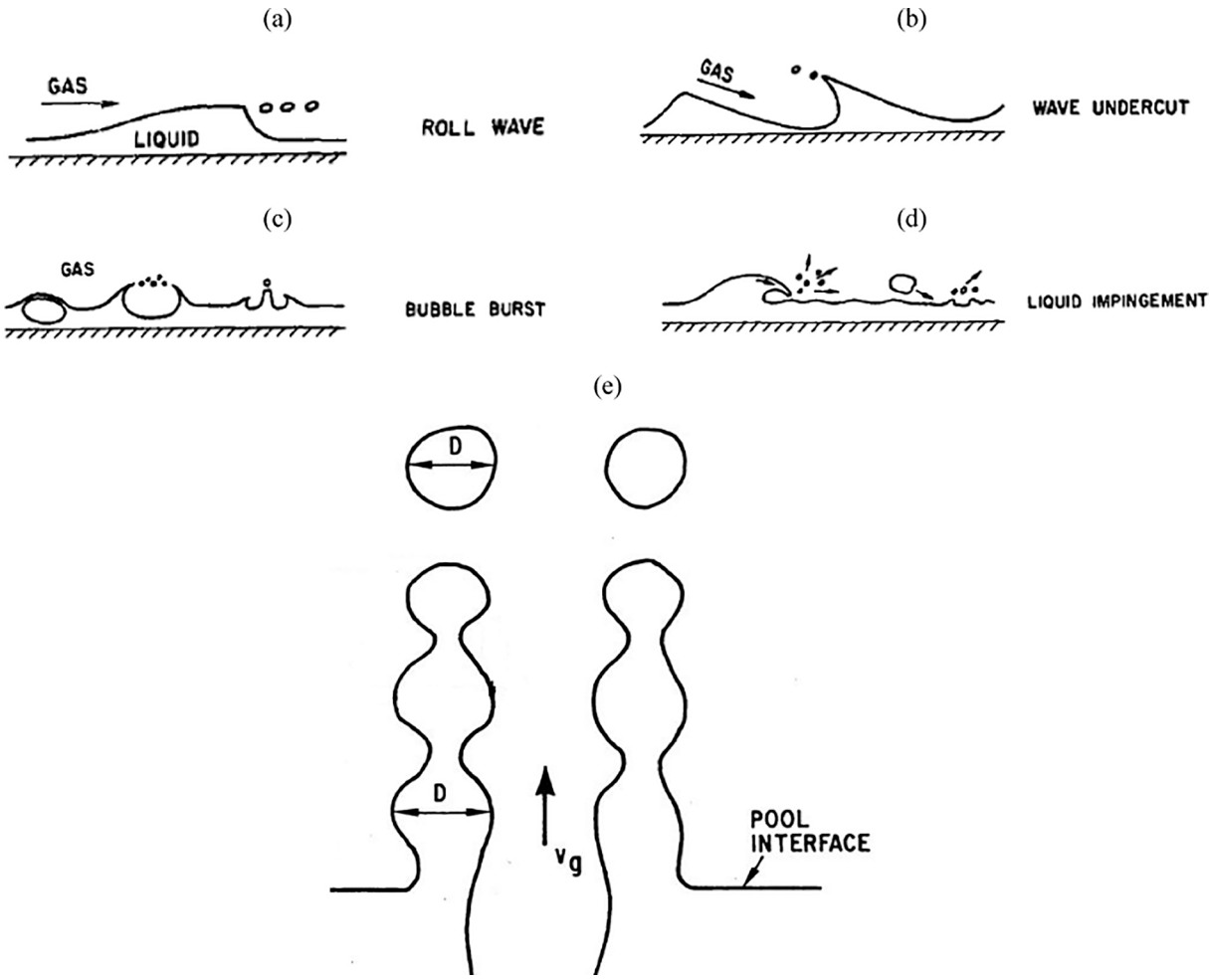

Fig. 2. Droplets generation mechanisms (de Santiago and Marvillet, 1991) (Kataoka and Mamoru, 1983).

current two-phase flow) occurs at infinite surfaces (such as the surface of the sea). This mechanism, as well, could be observed in stratified and annular flow regimes in pipes.

Entrainment occurs also from molten core concrete interactions MCCI. Consequently, large amount of steam and non-condensable gases are produced.

3. Review of modelling status

3.1. Pool scrubbing

Many pool scrubbing experiments have been conducted in the past, among them we mention the ACE experiments, the EPRI, General Electric Program, POSEIDON experiments, SPARTA experiments, UKAEA experiments, and JAERI experiments. A detailed description of the mentioned experimental programmes can be found in the report of Ramsdale et al. (1992).

The study of pool-scrubbing phenomena necessitates detailed investigation of pool hydrodynamics, and aerosol removal mechanism from injection to near the water surface. The driving forces are the key to understanding the aerosol retention mechanism. In the zone where the primary bubbles are formed, the condensation of steam with or without the presence of the non-condensable gases, the inertial impaction, Brownian diffusion and sedimentation take place. Computer codes are developed to quantify the retention of aerosols by means of the mentioned processes. Gao et al. (2017) showed in a comparative study various pool scrubbing codes (ART, BUSCA, SUPRA, SPARC-90 and SPARC-B/98), (Table 2). The table from Gao did not cover the updated version of BUSCA to BUSCA-PSI which was used to simulate the POSEIDON pool scrubbing experiments at PSI (Dehbi et al., 1994) as well as the ECART code. Table 2 below summarizes the aerosol removal processes considered in the codes.

When the gas is injected through the vent pipes, the Weber and the Bond numbers at the injection are significantly high, which means the globule formed at the inlet becomes unstable, loses its energy by breaking up, favouring another particle removal mechanism. This latter occurs each time when the bubble loses its energy. Then, depending on the size, particles could sediment or be intercepted by another bubble when this latter is rising. After leaving the bubble, the particles lose the ability to be transferred to other bubbles. Eventually, particles become trapped in the water pool. The breakup mechanism is considered in both BUSCA and SPARC codes.

Table 3 gives a summary of thermal hydraulics of the pool (Gao et al., 2017). BUSCA-PSI and ECART is added to it.

The bubble hydrodynamics depend on the thermal-hydraulics of the pool. In subcooled condition, the air bubbles rise as a function of gas injection velocity, from discrete bubbles (low gas flow rates) to size distributed bubbles (high gas flow rates). In saturated condition, water evaporates into the air bubbles as they rise due to hydrostatic pressure decrease. This bubble expansion affects droplet generation, as large bubbles reaching the pool surface contribute less in entrainment comparing to smaller ones.

In this frame, the IPRESCA (Gupta and Herranz, 2017) (Integration of Pool scrubbing Research to Enhance Source-term Calculations) project partners are conducting extensive investigation on implementing the removal mechanism under different flow regime, especially jet flow

regime. In addition, intensive work is being done to couple, aerosol removal mechanisms and bubble hydrodynamics.

In COCOSYS 2.4v4 (Arndt et al., 2015), the churn turbulent flow regime is not covered. The Decontamination Factor *DF* is calculated from the aerosol depletion efficiency *DEPEFF,* via the following equation $= \frac{1}{1-DEPEFF}$,

The rising cluster of bubble is log-normally distributed (Eq. (1)) in SPARC-90 code with two parameters, mean diameter and standard deviation in Eq. (2). SPARC-90 module implemented in COCOSYS, uses a correlation to calculate mean bubble rising velocity (Schmitz, 2000) as in Eq. (3) and Eq. (4):

$$f(d) = \frac{1}{log(\sigma_s)\sqrt{(2\pi)}} exp\left(\frac{-\left(logd_b - log\overline{d_b}\right)^2}{2(log\sigma_s)^2}\right) \quad (1)$$

$$\overline{d_b} = 0.72exp\left(2.303\left[-0.2265 + (0.0203 + 0.0313.x_{nc})^{0.5}\right]\right) \quad (2)$$

$$v_b = 7.876\left(\frac{\sigma}{\rho}\right)^{0.25}, d_b \leq 0.5cm \quad (3)$$

$$v_b = 1.40713\left(7.876\left(\frac{\sigma}{\rho}\right)^{0.25}\right) d_b^{0.4975}, d_b > 0.5cm \quad (4)$$

For pure non-condensable or steam-non-condensable gas bubble, SPARC-90 and SPARC-B/98 assumed that thermal equilibrium is reached immediately (Moody and Nagy, 1983). This assumption does not conform to the realistic condition when bubbles contain a mixture of steam and non-condensable gases because this latter may hinder steam condensation (Norman et al., 2006).

The Eq. (2) is the mean diameter for a steam-non condensable gas bubble. For a pure non-condensable bubble, $x_{nc} = 1$, the diameter is 0.72 cm. The presence of steam reduces this diameter due to condensation. For $x_{nc} = 0$, this diameter is 0.59 cm.

The bubble geometry and dynamics in the pool is a necessary information to analyse the entrainment phenomenon. At low and intermediate superficial gas velocity that conform to bubbly flow regime, the bubble can still be analysed since the geometry is known (Shah et al., 1982). In high superficial gas velocity that corresponds to churn turbulent flow, the bubble geometry cannot be identified.

3.2. Entrainment of water droplets

3.2.1. Theoretical work

Beginning with the bubbly flow regime, the bubble shapes range from spherical over elliptic to spherical cap (Clift et al., 1978). As shown in Table 1, the bubble trajectory from the injection to the water surface is not a straight motion: the buoyancy force and the interaction between bubbles yield a zig zag motion until they reach the water surface. The bubbles reach the surface to form a cap, or remain spherical in shape depending on their sizes (Toba, 1959), (Lhuissier and Villermaux, 2012). The capillary length indicates at which scale the gravitational and the surface forces are in balance (Poulain et al., 2018). It is an important magnitude when analysing the bubble burst at the water surface, however bubbles have multiple size and therefore multiple shape. Therefore, bubble stability is achieved by analysing the bubble Bond number equation (5).

$$Bo_{bub} = \frac{d_b g \Delta\rho}{\sigma} = \frac{d_b g \rho_g}{\sigma}\left(\frac{\Delta\rho}{\rho_g}\right) \quad (5)$$

Surface tension produces the centripetal force on the bubble lamellae sitting on the water surface. It is counteracted by the bubbles' internal overpressure. The bursting process is initiated by local thinning of the lamellae and hydrodynamic instability (Rayleigh–Taylor instability). Two families of drops are generated from the burst; film drops or film droplets produced from the bubble cap, and jet drops which are eventual consequences of film drops. The jet drops are produced from the agitation of the water liquid inside the bubble after the burst, caused by the bubble pressure, and the drained film into the water bulk.

The formation of the droplets in the interaction gas–liquid is a key to understanding mass and heat transfer between the phases (some problems include a third phase (soluble or insoluble particles).

The mechanisms of droplet generation (c, d and e of Fig. 2) are mostly encountered in large pools. In a vessel filled with water, the bubbles are produced either by boiling due to continuous heat release, depressurization, or by gas injection via vents. The swell level of the pool surface depends on the gas injection patterns and pool dimensions.

The cumulative water droplets generated from the bursting bubbles at the water pool surface are ejected with different sizes and velocities in a parabolic movement like a projectile. Spiel (1998a), Spiel (1998b) investigated the angle of ejection of film droplets burst at the centre, and found that the angles does not depend on the bubble size. Against the gas velocity, the droplets might settle down, or be carried over by the gas stream to eventually stay airborne at specific heights. In Stokes flow regime, the terminal velocity, which is the maximum velocity reached by the droplet as it falls back in the vertical direction, of the droplets larger than the gas velocity results in them settling down. With terminal velocity smaller than the gas velocity, the droplets continue to rise to the top vessel to stay volatile.

Sterman et al. (1957) summarize the dependence of entrainment on superficial gas velocity and height above the water surface for small values of Bond number (small pool diameter) as shown in Fig. 3 and Table 4.

Zenz and Weil (1958) developed a theoretical approach to quantify the entrainment of solid particle by a gas phase. Yeh and Zuber (1960) adapt their technique to calculate the entrainment for a liquid–gas system through drop dynamics above the liquid surface as a function of the initial drop velocity u_i' and the physical properties of the liquid and gas. However, a number of considerations were assumed to quantify the entrainment numerically;

First, the droplet sizes produced by the bubble burst or impingement follow a lognormal distribution, and are considered to be a number of bubble size classes. The physical properties of the operating system are constant and the initial droplet velocity is known (Davis, 1940) calculated this velocity assuming movement of a projectile, and balancing initial droplet kinetic energy and terminal potential energy $u_i^{'} = \sqrt{2gh_m} = 140cm/s$). The droplets are separated by the gas stream and carried away if the terminal velocity$v_t > 0$, and return back to the liquid surface if $u_t^{'} < 0$. The droplet velocity can be calculated as a function of

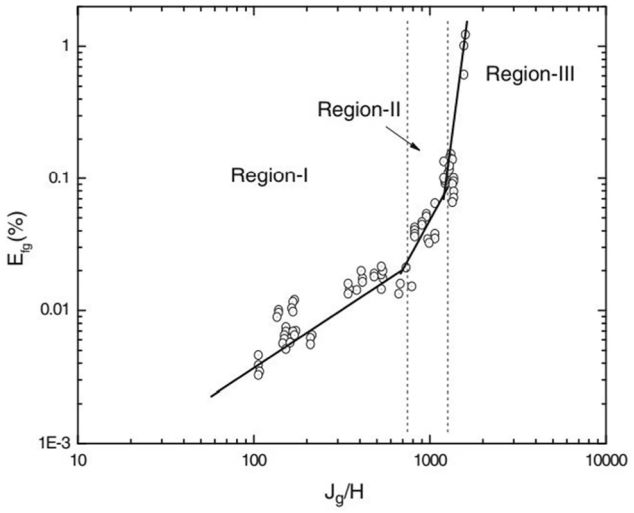

Fig. 3. Entrainment as a function of superficial gas velocity and height above the water surface (Sterman et al., 1957).

Table 4
Superficial gas velocity exponent with respect to zone above the water pool (Sterman et al., 1957).

Zone	I (near surface)	II (momentum controlled)	III (deposition)
n	$0 \rightarrow 1$	$3 \rightarrow 4$	$7 \rightarrow 20$
Condition for water droplet volatility	$v_t > j_g$	$v_t \leq j_g$	$v_t < j_g$

time from Eq. (6) (Zenz and Weil, 1958)(Yeh and Zuber, 1960).

$$u^{'} = v_t\left(1 - e^{\frac{-18\mu_g t}{\rho_l d_b^2}}\right) + u_i^{'} e^{\frac{-18\mu_g t}{\rho_l d_b^2}} \tag{6}$$

The height of rising droplets as a function of time can be calculated as per Eq. (7).

$$h = v_t t - \left(v_t - u_i^{'}\right)\frac{\rho_l d_b^2}{18\mu_g}\left(1 - e^{\frac{-18\mu_g t}{\rho_l d_b^2}}\right) \tag{7}$$

Finally, the entrainment of the droplets carried away is calculated. The numerical scheme proposed by the Zenz and Weil (1958) requires knowledge of the number of droplets produced by a bubble size and $u_i^{'}$ or j_g, which are already available from experimental works of Zhang et al. (2012), Koch et al. (2000) and de Santiago and Marvillet (1991).

Yeh and Zuber (1960) modified the work of Andrews (Andrews, 1960) on entrainment of fluidized solids to calculate the entrainment rate of droplets. Initially, Andrews assumed that entrained droplets need a sufficient amount of kinetic energy to escape. Gordon and Zuber added the following: a steady state must be maintained. The total energy of droplets remains constant. The number of particles must remain unchanged. All these assumptions match those of the kinetic theory; therefore, Andrews assumed that the energy distribution of droplets at the interface follows the Maxwell Boltzmann distribution law$f_i = \beta e^{-\beta\epsilon_i}$.

The entrainment rate of droplets (Eq. (9)) is obtained considering the inventory of droplets in the vessel (Eq. (8)) with kinetic energy$\epsilon_i = \frac{mu_i^2}{2}$.

$$\frac{dE_{fg}}{dt} = \frac{-A\rho_l u_i^{'} f_i}{6} \tag{8}$$

$$E_{fg} = \frac{1}{2\beta mg}\sqrt{\frac{\pi}{\beta mg}}\left[1 - \Phi\sqrt{\beta mgh}\right] + \frac{\sqrt{h}e^{-\beta mgh}}{\beta mg} \tag{9}$$

The entrainment rate developed by Andrews (1960) and modified by Yeh and Zuber (1960) does not depend on the gas velocity, it only gives information about the droplets' velocity distribution. The gas velocity changes the droplet size distribution, therefore, the entrainment rate as stated by Yeh and Zuber (1960).

However, the formulation of Andrews (1960) is evaluated at steady states. It is not the case in a containment building where the pressure increase as a consequence of non-condensable gases release in to the containment atmosphere.

Kruzhilin (1951) adopted a semi-empirical method to determine the entrainment, assuming that the contribution of the film droplets produced by the disintegration of the bubble cap is neglected. The droplets that contribute to the entrainment are those carried away by sufficient gas kinetic energy, and interaction between droplets is neglected. Therefore, the amount of entrained droplets depends upon the kinetic energy of the gas stream and physical properties of the liquid. Based on a dimensional analysis, Kruzhilin (1951) obtained the following:

$$E_{fg} = C_K\frac{\rho_g j_g^4}{\sigma g}\sqrt{\frac{\rho_g}{\rho_l}} \tag{10}$$

C_K is determined experimentally.

The effect of height is not considered in the formulation of Kruzhilin (1951), thus, his model is suitable to calculate the entrainment near the water surface. The correlation of Kruzhilin is limited, for the reason that the entrainment depends only of jet drops. This latter is large so it needs large gas kinetic energy to be entrained and carried over. The void fraction increase with increasing gas velocity, therefore, that implies the formation of large bubbles. It exists an upper limit for jet drop production for a critical bubble size (de Santiago and Marvillet, 1991), (Poulain et al., 2018), (Zhang et al., 2012).

Panasenko and Antonov (1959), later on, decided that the formulation of Kruzhilin (1951) needed to be re-evaluated and adapted it to their considerations. First, the complexity of the problem is increased by cancelling assumptions made by Kruzhilin (1951), (Yeh and Zuber, 1960). This implies introducing the height of the vapour space above the water surface. Kruzhilin's (1951) correlation is suitable for the second region, while the Panasenko and Antonov correlation is evaluated for the transition point (Fig. 3).

$$E_{fg} = 1.96{*}10^7\frac{\left(\rho_g g\right)^{0.48}\mu_l^{1.8} j_g^{1.96}}{g^{0.08}\left(\rho_l g\right)^{1.03}\sigma^{1.25}h^{1.18}} \tag{11}$$

Eq. (11) was correlated with experimental data of Sterman et al. (1957), Sterman et al. (1958) and Styrikovich et al. (1955)[1].

The height h is calculated from the volume fraction of the gas in the pool. However, his correlations are limited for pool diameter where the hydrodynamic effect and instabilities of the swell level of two phase flow are significant (Yeh and Zuber, 1960).

Sterman (1958) studied the effect of pressure on pool entrainment based on dimensional analysis. The equation (12) is based on previous experiments (Sterman et al., 1957), (Styrikovich et al., 1955), (Sterman et al., 1958), (Sterman, 1952) and (Kolokoltzev, 1952).

$$E_{fg} = 6,1.10^9\frac{\left(\frac{j_g}{gh}\right)^{1.38}\left(\frac{a}{h}\right)^{0.92}}{\left(\frac{ga^3}{\nu_l^2}\right)^{1.1}\left(\frac{\Delta\rho}{\rho_s}\right)^{1.124}}, \quad with \quad a = \left(\frac{\sigma}{g\Delta\rho}\right)^{0.5} \tag{12}$$

The parameter h in Eqs. (11) and (12) is the height of the vapour space, from the water surface to the top vessel, and depends on the gas volume fraction. This height decreases with increasing gas flow rate. Sterman (1958) in his correlation adopted a formulation for gas volume fraction Eq. (13) which depends upon gas velocity (Sterman, 1957).

$$\alpha = 0.26\left(\frac{j_g^2}{g\sqrt{\frac{\sigma}{g\Delta\rho}}}\right)^{0.4}\left(\frac{\rho_g}{\Delta\rho}\right)^{0.12} \tag{13}$$

Under the condition:

$$Bo \leq 260\left(\frac{\rho_g}{\Delta\rho}\right)^{-0.2}$$

For an air–water system at Sterman's conditions (Sterman et al., 1957) (P = 185 atm and pool diameter d = 0.255 m): $Bo = 287.25 < \left[260\left(\frac{\rho_g}{\Delta\rho}\right)^{-0.2} = 357.30\right]$

Golub (Rozen et al., 1970) considered a normal law to describe the droplet size distribution, and analyse the entrainment from the forces applied to a single droplet; weight, buoyancy and drag. Then, he validated the model against experimental data to find the following relationship (Eq. (14)):

$$E_{fg} = \left[A.K^{0,5} + B.K^{2,1}\right]\sqrt{\frac{\Delta\rho}{\rho_g}}e^{-0,23h/D_H} \tag{14}$$

[1] These data are found in the Appendix of Yeh and Zuber work (Yeh and Zuber, 1960).

With $A = 9,011.10^{-5}\Delta\rho^{0,625}\rho_g^{-0.25}\sigma^{-0,375}g^{-0,25}$

$B = 0,753\Delta\rho^{1,025}\rho_g^{-0.5}\sigma^{-1,575}g^{-1,25}$

$K = d_{dr}j_g$

Reed's Correlation (Eq. (15)) (Westgarth, 1964) is obtained from the paper of Paradissiadis and Widmer (1984).

With

$$E_{fg} = \frac{R}{1-R}$$
$$with\ \ R = 284\left(\frac{n_g 10^6}{\rho_g\Delta\rho}\right)^2\left(\frac{j_g\rho_g}{3,23h^2+8,86h^2+3,6}\right) \quad (15)$$

Azbel (1981) proposed an entrainment equation based on a stochastic approach by assuming the flowing: the velocities of droplets and their size at the interface of the pool are independent, and the distribution of droplet velocities and their size obey a Gaussian distribution.

$$E_{fg} = E_0\left(\frac{1}{\sqrt{2\pi}}\int_b^0 exp\left(\frac{-x^2}{2}\right)dx + \int_0^\infty exp\left(\frac{-x^2}{2}\right)dx\right) \quad (16)$$

With $b = \frac{\sqrt{2gH}-V_0}{\sigma}$

The first integral term refers to the entrainment near the interface that corresponds to a specific height H, and the second integral term refers to the entrained droplet far from the surface, with velocity superior to the initial one at the time of the ejection. The Eq. (16) shows that with increasing height x, the entrainment decreases. That is consistent with the definition stated by Kataoka and Ishii; however, the Azbel model only indicates that entrainment is a function of height.

Kataoka and Mamoru (1983) developed a mechanistic model that includes three equations corresponding to three zones above the water pool, as shown in Table 4.

The first zone and the second zone are controlled by the momentum of the droplets, and the third zone is controlled by the deposition. Thus, from Kataoka's perspective, the entrainment of the droplets decreases as the distance to the water surface increases and as the gas velocity also decreases. In other terms, $h^* \gg j^* implies, \frac{j^*}{h^*} \to 0 so, E_{fg} \to 0$.

These zones are determined by analysing the main parameters having notable effect on entrainment. Kataoka and Ishii's considerations on quantifying the entrainment are different from previous work (Sterman (1958), Panasenko and Antonov (1959), Styrikovich et al. (1955) and Kruzhilin (1951)). Assuming that the droplets travel in a vertical direction – from zone I to zone III – gives rise to another parameter affecting the entrainment, which is the height above the water surface. The height itself depends on the composition of the atmosphere and pool's thermal hydraulics (Cosandey, 1999).

The Kataoka's (Kataoka and Mamoru, 1983) correlations for different regions above the water pool from the surface to the uppermost part of the vessel are:

For the near surface region $E_{fg}\left(h, j_g\right) = 4,84.10^{-3}\left(\frac{\rho_g}{\Delta\rho}\right)^{-1,0}$ (17)

Momentum controlled region

Low gas flux $E_{fg}\left(h, j_g\right) = 2,213N_{\mu g}^{1.5}D_H^{1,25}j_g^{*}h^{*-1}\left(\frac{\rho_g}{\Delta\rho}\right)^{-0,31}$ (18.1)

Intermediate gas flux $E_{fg}\left(h, j_g\right) = 5,417.10^6 j_g^{*3}h^{*-3}N_{\mu g}^{1.5}D_H^{1.25}\left(\frac{\rho_g}{\Delta\rho}\right)^{-0,31}$ (18.2)

High gas flux $E_{fg}\left(h, j_g\right) \propto \left(\frac{j_g^*}{h^*}\right)^{7\ 20}$ (18.3)

Deposition controlled region $E_{fg}\left(h, j_g\right) = 7,13.10^{-4}j_g^{*3}N_{\mu g}^{0.5}\left(\frac{\rho_g}{\Delta\rho}\right)^{-1,0}e\left(-0,205\left(\frac{h}{D_H}\right)\right)$ (19)

Eqs. (17)–(19) was validated against data of Styrikovich et al. (1964), Garner et al. (1954), Sterman et al. (1957), Sterman (1958), Styrikovich et al. (1964), Golub (1970) and Rozen et al. (1976b).

Cosandey (1999), Cosandey and Von Rohr (2001) developed a correlation to quantify the re-entrained soluble and insoluble particle under very low gas flow rates as a consequence of vessel slow depressurization, using data from their own experiments. The correlation is based on the dimensional Buckingham theory, which leads to a group of dimensionless numbers.

$$E_{fg} = k_1 x_{BP}^{k_2} We_{cont}^{k_3} Fr_{cont}^{k_4}(1+Ra)^{k_5} \quad (20)$$

The k_i, with $i = 1\cdots5$, are coefficients to be determined with experimental data (Table 5).

The limitation of the Eq. (20) is discussed in detail in Section 6.

Bagul (Bagul et al., 2018a) performed a CFD simulation to quantify the carryover through the exit of the steam drum using OpenFoam v2.3.1. Lagrangian method was used to track the droplet trajectories in the Eulerian phase (gas). The waving of the swell level (two-phase flow level) is expensive to simulate numerically, so for this reason Bagul simulated only the gas space above the water pool (Eulerian phase which is the distance between the swell level and the drum exit). The droplets were injected as discrete Lagrangian phase at different mass flow rates at the inlet. As the droplets are the main concern, the mesh was refined in the outlet zone and at the exit of the drum. It was found that, CFD simulation with high flow rates agrees with experimental data and Kataoka's model for low swell levels of up to 1.75 m. Beyond 1.8 m, Kataoka's model is valid for the range of superficial gas velocity as shown in Fig. 4. The results are far from being in agreement with CFD data, and that is due to the unrealistic conditions adopted during the simulation regarding the fixed swell level used instead of the oscillated one (realistic). In addition, the disagreement is due to the deposition of the droplet into the wall at the exit of the drum.

Bagul et al. (2019) performed another numerical simulation of the carryover and the droplet motion above the water surface for various heights. A 1D code was used which adopts several assumptions applied to the droplets ejected from the water surface. These assumptions match those of the Stokes flow regime. The droplets are perfect rigid spheres so the volume could be calculated easily. Also it is a 1D code, which means the ejected droplets have one direction in which to travel: from normal to water surface (droplets coalescence is not considered – because the superimposition of droplets will result in returning them to the water pool – and nor is the evaporation of droplets considered (Kataoka, and Ishii also adopted the same assumption)). Droplets have the same size, and the gas has constant velocity.

Bagul's data agree well with the correlation of Sterman (1958) and Kataoka and Mamoru (1983). The distance between the swell level and the drum exit is too small (0.2 m), and this corresponds to two zones (zone I and zone II in Table 4, which means the data agree with Kataoka's near surface entrainment equation (Eq. 17) and momentum controlled region equation (Eq. (19)). As shown in Fig. 5, the entrainment consists of all droplets (Kataoka and Mamoru, 1983). The movement of the droplets is accelerated passing the exit of the drum. Kruzhilin's correlation (Kruzhilin, 1951) does not depend on the height above the pool, and corresponds to zone I (Table 4). Therefore, it would agree with Bagul's experimental and numerical data. The correlations developed by Kruzhilin (1951) did not quantify the entrainment for a specific zone. Therefore, from Bagul's experimental data (Bagul et al., 2018a), it could be concluded that Eq. (10) is suitable for entrainment

Table 5
Coefficient k_i of the Eq. (5) to predict the entrainment for soluble and solid particles.

	k_1	k_2	k_3	k_4	k_5
Soluble fission product	2.954.10^{-9}	0.3636	1.1968	−1.3057	−0.0216
Solid fission product	0.095	0	−0.0997	0.0153	0.006

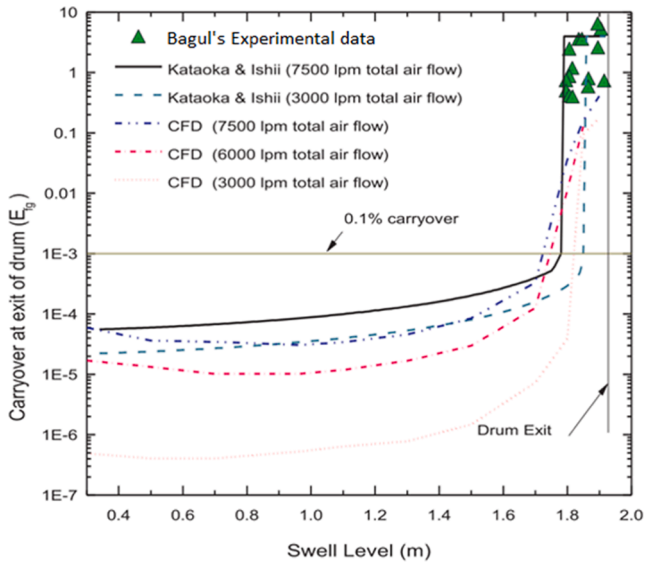

Fig. 4. Comparison of prediction of carryover by E-L simulations, correlations and experimental data (Bagul et al., 2018b).

near the surface region.

Lu and Xie (2017a), Lu and Xie (2017b) investigated numerically the phenomena of the water carry-over based on Kim's experiments (Kim and No, 2005a, 2005b) with an emphasis on the effect of the exit using an upward and a side exits. The performed simulation shows that a VOF model implemented in Ansys 16.0 Fluent showed effectiveness in simulating the pool entrainment, relative to Kim's experiments.

The mesh used in Lu and Xie simulation was limited in terms of the number of elements. The entrainment of water consisted of all droplet sizes – from those measured in *microns* to *mm*– and the elements have to be small enough to track such tiny droplets, (the element has to be one order of magnitude smaller than the droplet). Therefore, Lu (Lu and Xie, 2017b) in his work, did not consider small elements in the range of microns, since such simulation demands high computational performance as well as being time consuming. Therefore, the contribution of tiny droplets to the entrainment is neglected; however, it is not the case for different geometry where the height above the water pool is significant. Obviously this statement is applicable to such geometries as investigated by Kim and No (2005a), Kim and No (2005b) where

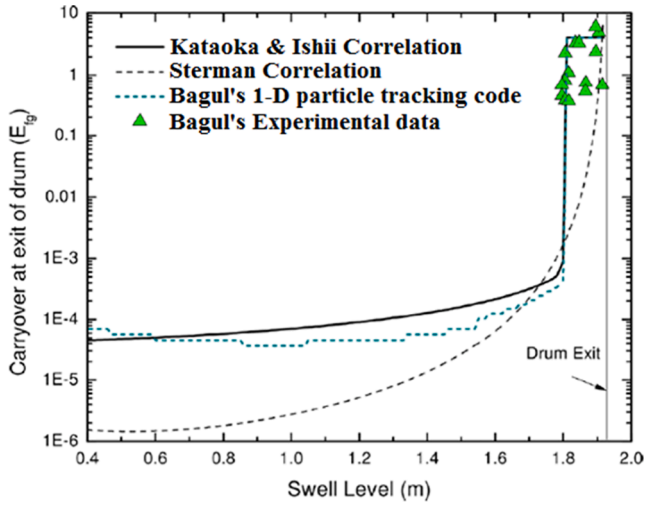

Fig. 5. Prediction of entrainment using 1D code and comparison against (Bagul et al., 2019) data and (Kataoka and Mamoru, 1983) and (Sterman, 1958) correlations.

entrained water is dragged through the exit, the velocity is significant (Bernoulli's effect). Therefore tiny droplets contribute less to the entrainment in that case, meaning that some of them will be deposited onto the wall exit, and that some of them will be added to the entrained water. Lu and Xie (2017b) assumed this could be neglected and reduce the number of elements to speed up the simulation. Kim and No (2003) used a cylindrical vessel in his experiments, while Lu and Xie (2017b) used a rectangular vessel in order to increase mesh quality.

The carry over using a side-exit is greater that the carry over calculated by the upward-exit (Fig. 6).

On one hand, for an upward exit, the water might accumulate at the exit, therefore due to gravity, it returns to the surface. On the other hand, this does not occur at the side exit, thus, even if the water accumulates at the exit, it will be laying at the lower side of the exit, and eventually will be driven out due to the Bernoulli effect. This effect itself could entrain droplet by roll wave as shown in Fig. 2.

4. Experimental work

4.1. Bubble burst and droplets generation

After rising, the bubbles sit on the surface, to eventually burst at any moment. Poulain et al. (2018) investigated this phenomena in detail for an air–water system. They examine the effect of temperature on ageing first, by producing discrete bubbles in a stainless steel tube from an air pump. They controlled the temperature (between 5° to 90 °C) by putting coiled tubing connected to a recirculating water heating or cooling pump which is wrapped around the tube. As water temperature increase the bubble ageing time decreases.

Moreover, the effect of surfactants on the life time of the bubble was examined by Poulain et al. (2018). The diffusion of soluble surfactant blob of a specified size across the film of a certain thickness initiates the Marangoni effect, and a perturbation of that surfactant blob could rupture the cap if the size of the blob is twice as bigger as the cap thickness. The surfactant in a bubble cap of size d_b diffuses from one side of a film of thickness h_f to the other side over time $\tau_{diff} h^2/D$.

Zhang et al. (2012) considered a dimensionless approach to studying the characteristics of droplets for several liquids. They developed correlations to predict the critical bubble size as a function of the physical properties of the liquid Eq. (21) and the number of produced jet drops (Eq. (22)).

$$d_{cr} = 10^{0,1914} \sigma_l^{0,5517} \rho_l^{-0,4830} g^{-0,5170} \mu_l^{-0,0688} \tag{21}$$

$$n_{dr} = 7,9e^{\left(\frac{-d_b}{0,338 d_{cr}}\right)} - 0,41 \tag{22}$$

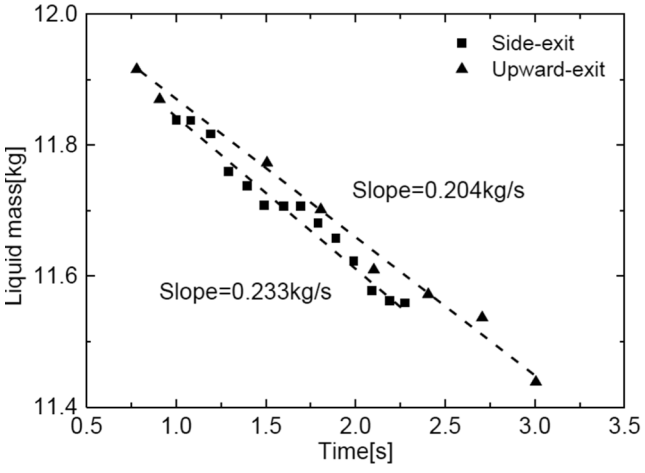

Fig. 6. Liquid mass loss rate for side exit and upward exit.

From Eq. (22), the number of the jet drops depends on the bubble size. For significantly large bubbles, practically no jet drop is produced, and the only drops that can be generated from such bubbles are from the thin film form at the surface $n_{dr} \rightarrow 0$ as can be seen in Fig. 7.

As Eq. (21) shows, the critical bubble size where no jet droplet is produced, depends on properties of the liquids. It increases for fluids with low density and low viscosity. When the bubble is resting on the fluid surface, it is submitted to two forces: surface tension, and centripetal forces, assuming no interactions with its surroundings. The bubble will burst under the condition (Spiel, 1998a, 1998b);

$$\frac{M_1 S_f^2}{R_0} > 2\sigma$$

Therefore, the critical bubble size, in Eq. (21) increases when surface tension increases. This equation resulted from a dimensionless and regression analysis, considering a combination of the

Froude number, the Reynolds number and the Weber number and plots it against the Morton number. The combination of Re, Fr and We were made in order to cancel the velocity term, so it eventually yields the critical bubble size.

Above this size, practically no jet drop is generated as is shown in Fig. 7. The number of drops increases for bubbles 20% smaller than the critical bubble size, and this decreases exponentially.

The experiment of Zhang et al. (2012) is relevant to quantify the droplet entrainment for pure and contaminated water. As demonstrated, high fluid viscosity, produce fewer droplets. Toba (1959) and Spiel (1998a), Spiel (1998b) used sea water to investigate the number of droplets, under T = 10 °C and T = 28 °C respectively. More droplets was produced under Spiel condition (Spiel, 1998a, 1998b) than Toba (1959). Concluding that droplets production increase with decreasing temperature accordingly.

The drops generated by bubble whether from film or from jet contribute to the entrainment taking into account the bubble size, flow regimes hence interaction between bubbles.

Such droplet might be entrained by the streaming gas to different location above the water pool. Kataoka and Ishii, subdivided these location into three regions: 1) near the surface where the entrained droplets consist of all sizes, 2) the momentum controlled region which is considered as the transition region where droplets are either carried over or fall back, and 3) the deposition controlled region where droplets are small enough to be carried over and suspended, unless deposited onto wall. Some authors conducted experiment to quantify the entrainment of droplet in the momentum controlled regions, and others

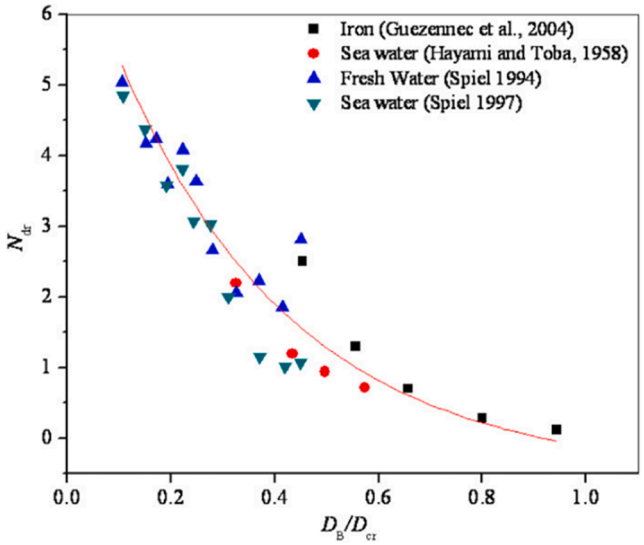

Fig. 7. Zhang's correlation (Zhang et al., 2012) against experimental data.

conducted experiment to measure the entrainment in the deposition controlled region. The near surface region is a challenging zone to measure the entrainment due to high water surface agitation from multiple bubble burst. However, since the entrainment consists of all droplet at the near surface region, Kataoka and Ishii, stated that the droplets mass flux is 4 times larger than the gas mass flux. This value is validated by previous authors as well.

Experiments on water entrainment could be conducted in large and small vessel. As for large vessel, it could be attributed to the containment building (where entrainment is measured in the deposition controlled region) while small vessel corresponds to scenarios such as SGTR, SBLOCA (where entrainment is measured in the momentum controlled region).

4.2. Entrainment

Experiments on water entrainment could be subdivided into large pool entrainment and small pool entrainment. As for large pool, it corresponds to the containment building, while small pool diameter corresponds to scenarios such as SGTR, SBLOCA.

Kudo et al. (1994) experimentally investigated the aerosols release from the water surface by entrainment of water droplets from flashing pool in the frame of the ALPHA program in a BWR Mark 1 containment.

The facility was a model containment vessel with 3.9 m of inner diameter and 5.7 m of height, and a volume of 50 m^3. Inside the vessel was placed a 2 m deep steel water pool. For the depressurization, was used a discharged pipe equipped with a valve and a condensation tank that connect the containment vessel by the pipe. The opening or the breach area of the containment during the flashing was simulated by scaling the containment volume and the containment breach size.

Two experiments were conducted and the differences between them are the water mass in the pool and the mass of dissolved sodium sulphate.

Three samplings were taken, and as a result, the size distribution of the airborne aerosols was surprisingly bimodal for some samplings as shown in Fig. 8. Kudo et al. (1994) stated that the reason is not clear and the generated droplet mechanisms might be one of the explanations, which is a consequence of the rate of the depressurization and the position of the vent.

In both experiments, the superficial gas velocity was below 0.04 m/s. Mass entrainment from the pool at the surface measured does not agree with Kataoka's model. Kataoka and Ishii assumed that the pool bubbles in a uniform fashion. The scenarios under which the pool could bubble in a uniform fashion are the flashing pool under low depressurization rates (which is enough to generate bubbles across the entire pool surface,) or a well distributed quencher in such way to make the entire pool bubbles.

Kudo's experiments show an increase of superficial gas velocity near the walls, and a decrease towards the centre of the pool. Therefore churn turbulent flow is near the walls and bubbly flow is in the centre as observed by Kudo. The velocity profile might be described as a parabolic. The depressurization scenario obviously is not steady state, and Kataoka's model considers a steady state data to develop his correlation. That explains the discrepancy between the measured entrainment and Kataoka's model.

Kim and No (2003), (Kim and No, 2005a, 2005b) conducted experiments on pool entrainment to simulate the depressurization system of Advanced Power Reactor 1400 in the case of TLOFW. The facility consisted of a pool and a break at the top to measure the amount of water droplets. Kim and No's data were compared against previous work of Rozen et al. (1970), Sterman (1958) and Styrikovich et al. (1964). None of them agree with Kim's experimental data, and the measured entrainment was much higher than the previous measured data (Fig. 9). The reason behind this deviation is discussed in the last section of this paper.

Kim adapted the Kataoka's model to experimental data in order to

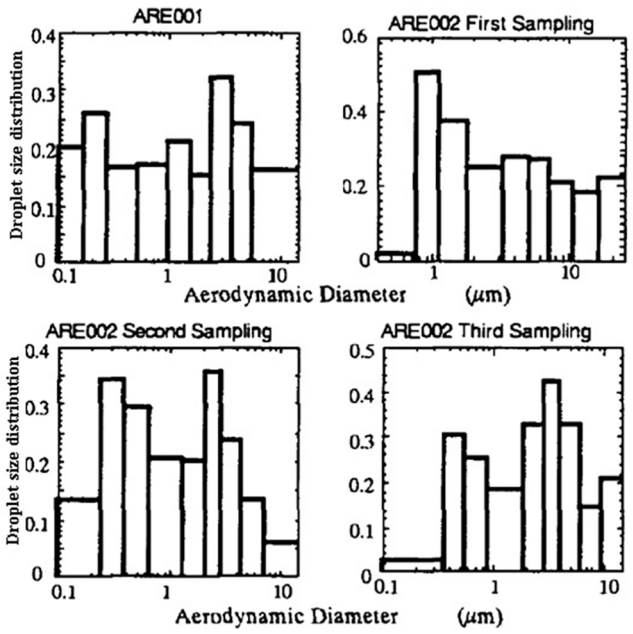

Fig. 8. Size distribution of airborne droplets (Kudo et al., 1994).

ascertain a correlation, which depends on superficial velocity to 7th power, as could be seen in Eq. (23). That is due to substantial momentum in the top break – as shown in Fig. 10– with the entrainment in that case being a strong function of the ratio of the break diameter to the distance between the water surface and the break, along with the gas superficial velocity.

$$E_{fg} = 7,706.10^{20} j_g^{*7} h^{*-7} \tag{23}$$

Aerosol release by droplet entrainment was extended to a non-Newtonian fluid/gas system. The complexity of treating non-Newtonian fluid lies in the physical properties of the liquid, and more precisely, the viscosity. This latter is no longer assumed constant, but is a function of the shear stress. The behaviour of the fluid depends on the shear stress, and it has a threshold value where the non-Newtonian fluid behaves like a Newtonian fluid. Fritz (2006), simulated the radioactive wastes from the Hanford site in Washington that are stored in underground tanks. The clean-up strategy is to retrieve the liquid slurry waste from the tanks and stabilize it by glassification at a Waste Treatment Plant (Gephart and Lundgren, 1995). The experiment was conducted in a half-scaled tank filled with a waste simulant processing Bingham plastic rheological properties (Fig. 11) which is similar to the expected properties of the nuclear waste. The simulant consisted of a mixture of 80% kaolin clay and 20% bentonite clay mixed with water. Filtered air was used as injected gas via 9 spargers under different flow rates. The entrainment was measured in three different heights above the liquid surface (Kataoka and Mamoru, 1983). The measured entrainment was compared for the bubbly flow regime with the Rozen correlation (Rozen et al., 1976a) and Kataoka's model in the momentum controlled region. Fritz adapted the Kataoka's model for the deposition region to the bubbly flow regime, by reducing the exponent of the superficial gas velocity from 3 to 1, as can be seen in Eq. (24).

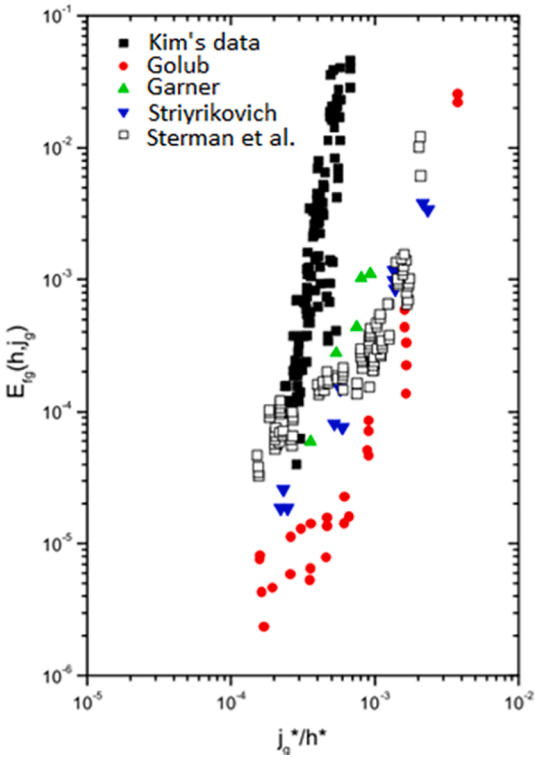

Fig. 9. Comparison of the experiment of Kim, Hyun and No, Cheon (2005) and previous experimental works.

$$E_{fg}(h, j_g) = 7,13.10^{-4}(0,025) j_g^{*} N_{\mu g}^{0.5} \left(\frac{\rho_g}{\Delta\rho}\right)^{-1} e\left(-0,205\left(\frac{h}{D_H}\right)\right) \tag{24}$$

As for the Rozen's formula, the entrainment agrees with experimental data for the momentum controlled and deposition regions (Fig. 12). Rozen's correlation is as accurate as the modified Kataoka equation. The lack of efficiency of the aerosol samplers resulted in a disagreement with the Kataoka and Ishii model for the momentum controlled region. However, the modified Kataoka's model for the deposition controlled region under bubbly flow agrees with experimental data. The entrainment of droplets in non-Newtonian fluid system cannot be applied to high superficial gas velocity for the behaviour of the viscosity (the resistance to the gas motion).

The modified Kataoka (Fritz, 2006) and Rozen et al. (1970) correlations and the measured entrainment show no dependence on sampling height above the water pool in the deposition-controlled region. It was also observed in previous THAI experiments (TH25), as shown in Fig. 13. The entrainment measured at H = 6.5 m is similar to the entrainment measured at H = 7.7 m. The zone is considered uniformly distributed; therefore, the entrainment is the same at every point in the deposition-controlled region for a given gas velocity value.

Bagul et al. (2018a) simulated experimentally the AHWR heat transport to drums, where steam is transported and condensed in the scaled down, Air Water Loop AWL facility. The entrainment was measured near the surface, close to the drum exit. This is equivalent to the pool entrainment near the surface and in the momentum-controlled region. This is due to the swelling level of the two-phase mixture, which limits the gas space. The experimental results successfully validated the previous mechanistic models and correlations of entrainment for high swell level. This later has to be high enough to capture an important amount of droplets. That is conformed to Kataoka's statement that entrainment at near surface consisted of all droplets, and that the mass flow rate of the entrained liquid is 4 times the gas flow rate. In Fig. 14, the measured entrainment agrees with Kataoka's, and Sterman's models. Sterman's correlation is a non-linear function asymptotic to the exit of the drum, meaning that the entrainment increases infinitely. However, the experimental data lies between these two models.

The experiments of Kim and No (2003) (discharge pipe *50 mm, 5 mm* -holes injection) and Bagul et al. (2018a) (Drum exit *102.26 mm*) are similar as regards the entrainment mechanisms, however there are still some differences in the boundary conditions, as could be seen in the Table 6 below.

Kim used high air flow rate, and the distance from the swell level to

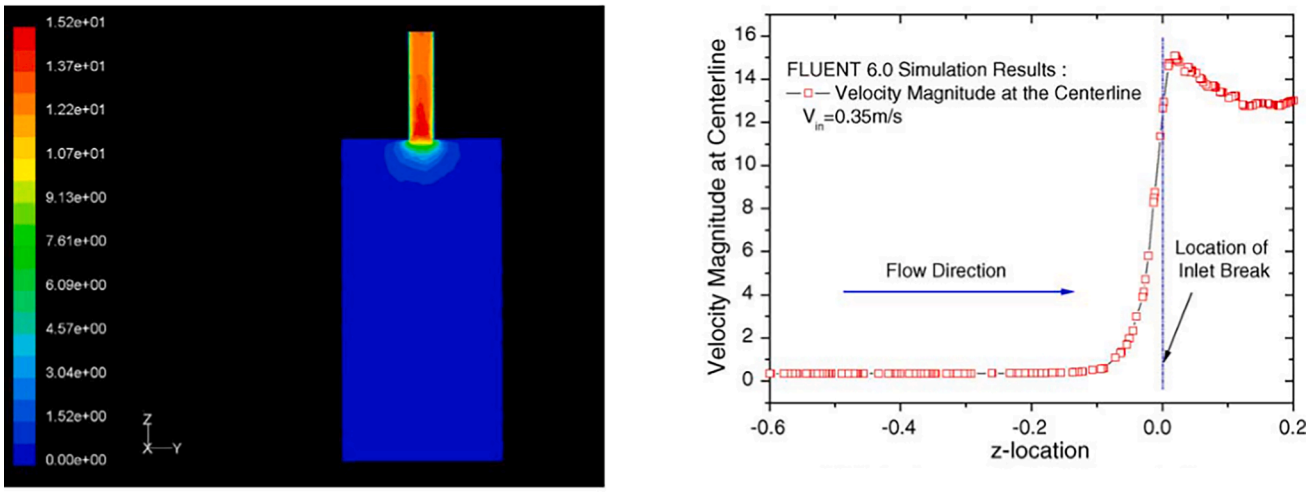

Fig. 10. CFD simulation showing velocity contour (right), velocity profile at the center vertical line (left).

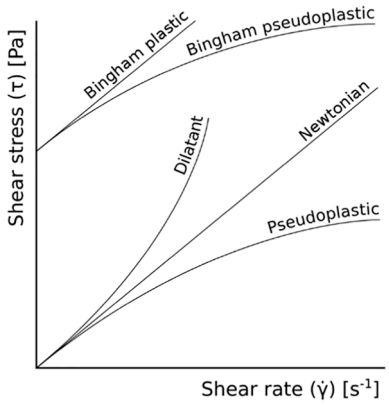

Fig. 11. Classification of fluids with shear stress.

the break was from 0.4 m to 0.1 m. While in Bagul's it was no less than 0.015 m, which is very close to the exit, allowing more droplets to be entrained. Even so, Bagul's experiments showed higher values of liquid entrainment than those of Kim's. That could be explained as follows: the height above the pool for Kim is much higher than in the Bagul experiment, even if Kim and No (2005a), Kim and No (2005b)a) used higher superficial gas velocity, the Bernoulli Effect is more significant in Bagul experiments.

It is worthwhile comparing Kim's and Bagul's experiments with previous data (Sterman experiment (Sterman et al., 1957) and Styrikovich et al. (1955)) to understand the discrepancies. The disagreement is due to the following: Sterman (1957) developed an equation for the volume gas fraction above the two-phase flow mixture to calculate the height of the vapour space h during bubbling (Eqs. (25), (26)):

$$\alpha = 0.26\left(\frac{j_g^2}{g\sqrt{\frac{\sigma}{g\Delta\rho}}}\right)^{0.4}\left(\frac{\rho_g}{\Delta\rho}\right)^{0.12} \tag{25}$$

$$h = H - \frac{h_l\alpha}{1-\alpha} \tag{26}$$

Thus, the distance h as a function of thermal hydraulic condition of Sterman experiment (Sterman et al., 1957) and Styrikovich et al. (1955) could be calculated from Eq. (26). Kim and No (2003) deduced this value experimentally.

This means that the Sterman's model to calculate the gas volume fraction is valid (Sterman, 1957).

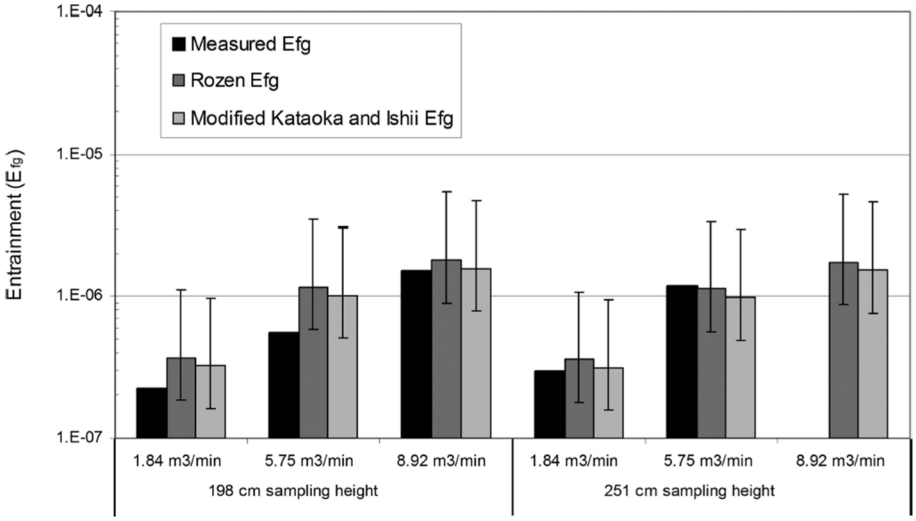

Fig. 12. Comparison of measured entrainment and modified Kataoka and Ishii correlation (Fritz, 2006) and Rozen correlation (Rozen et al., 1976b) in the deposition controlled region under a bubbly flow regime.

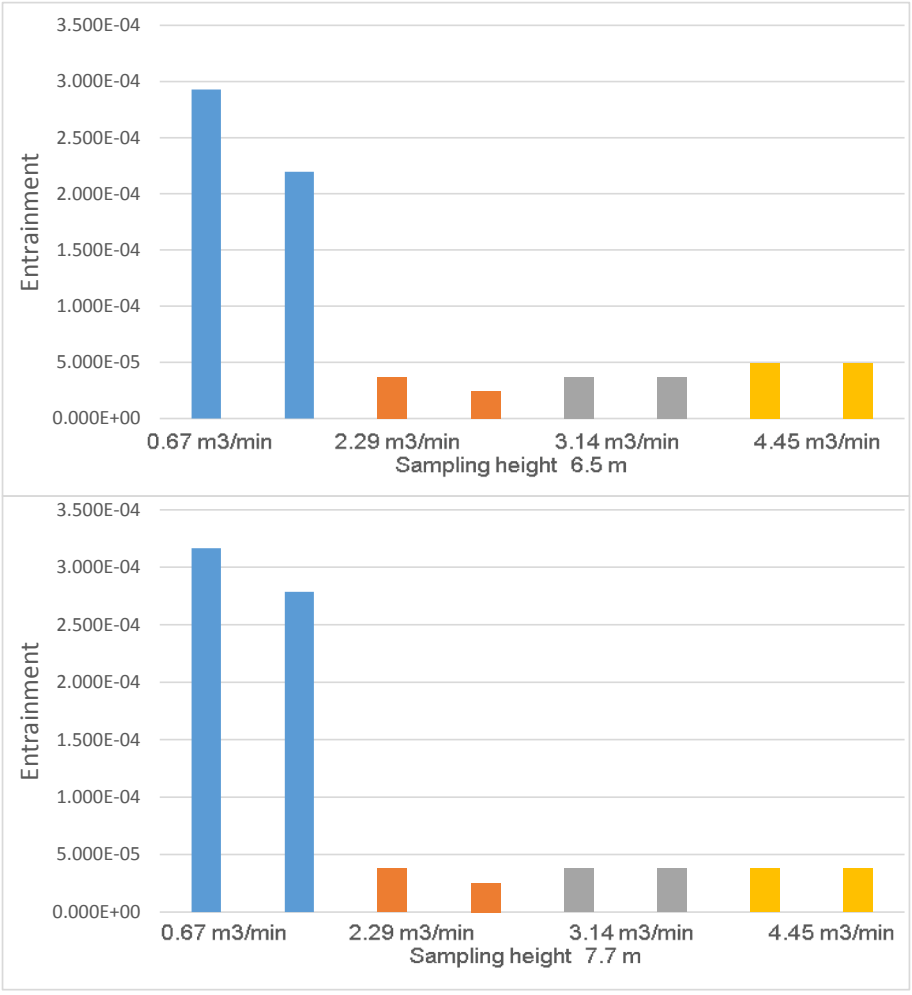

Fig. 13. Entrainment measured in TH25 THAI experiment.

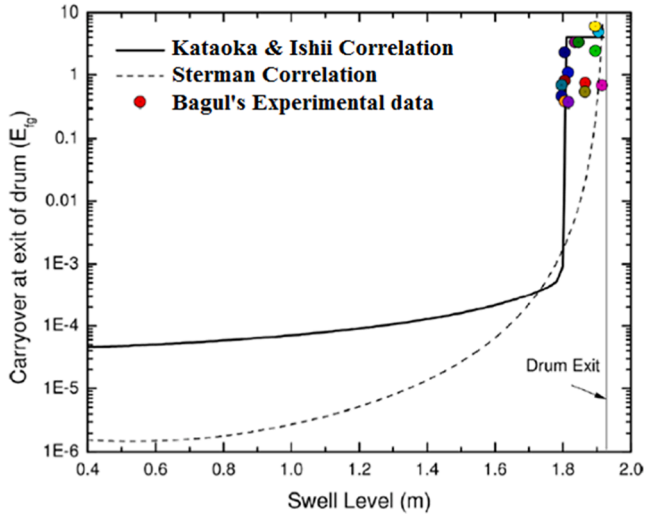

Fig. 14. Comparison between entrainment measurement (Bagul et al., 2018a) and Kataoka & Ishii and Sterman correlations.

Table 7 shows a comparison between Kim and No (2003), Bagul et al. (2018a), Sterman et al. (1957) and Styrikovich et al. (1955) data on water carry-over. First, the criterion to compare these results is that the condition $Bo \leq 260\left(\frac{\rho_g}{\Delta\rho}\right)^{-0.2}$ has to be fulfilled. From Table 7, as the superficial gas velocity increases, the height of the gas space above the two-phase flow level decreases, therefore the entrainment increases due to Bernoulli's effect at the exit.

Table 6
Comparison of Bagul's and Kim's experiments.

	Bagul experiments	Kim experiments
Superficial gas velocity [m/s]	0.099 – 0.277	0.01 – 0.35
Two phase flow level [m]	1.798 – 1.915	1.0 – 1.9
Entrainment [–]	0.371 – 4.900	1E-1 – 7
System	Air – water	Air – water
Temperature [°C]	Atmospheric	Atmospheric
Pressure [bar]	Atmospheric	Atmospheric

Ramirez (de Santiago and Marvillet, 1991) in the frame of PhD work, also investigated experimentally the phenomenon of pool entrainment, with an emphasis on the droplet size and velocity distribution. The performed study focused on the droplet entrainment at different height above the water pool for superficial gas velocities in the range [0.13 m/s – 0.4 m/s] using a 108 *mm* pool diameter. It was found that the gas velocity have a clear impact of the droplet size distribution in the deposition controlled region. In this region, the droplet are either entrained or deposited due to advection for small pool diameter. The study of Ramirez (de Santiago and Marvillet, 1991) does not apply to large pool diameter. However, the approach adopted gives some interesting insight to model entrainment in large pool diameter.

Table 7
The effect of the height of the vapour space in a bubbling pool and superficial gas velocity on entrainment.

	j_g(m/s)	h_{fg}(m)	h(m)	E_{fg}(\%)∨
Bagul et al. (2018a) P = 1atm	0.099 – 0.277	1.798 – 1.915	0.122–0	0.371 – 4.900
Kim and No (2003) P = 1atm	0.09 – 0.33	1.0 – 1.9	1.0–0.1	0.01 – 0.1
Sterman et al. (1957) P = 151atmP = 185atm	0.166 0.075	0.2537 0.244	0.5663 0.4060	0.12% 0.06%
Styrikovich et al. (1955) P = 36atmP = 91atm	0.524 – 0.535 0.260 – 0.266	0.3668 0.2819	0.4782 0.5631	0.1% 0.04%

5. Discussion

The experiments are the key to unlocking the variable responsible for a specific phenomenon. The entrainment from water pools has been investigated for different scenarios: entrainment obtained by gas release from the surface of the pool by gas injection (downcomer, quencher, horizontal vent), (Freitag and Schmidt, 2017), (Kim and No, 2005a, 2005b), (Bagul et al., 2019), and entrainment measured by depressurization (Kudo et al., 1994), (Freitag and Schmidt, 2017).

Authors, (Kataoka and Mamoru, 1983), (Rozen et al., 1976a), (Styrikovich et al., 1964) and (Kruzhilin, 1951), (Cosandey, 1999) developed theoretical and semi-empirical correlations, and empirical correlations, (Kim and No, 2005a, 2005b). From these correlations, we may deduce variables that affect the entrainment.

The analytical formulated by previous athors presented in this chapter attempted to give a prediction of the entrainment of water droplet, however, some formulation needed data to be validated, and others showed applicability limitations.

The equation of Zenz and Weil (1958) is a satisfactory theoretical approach only if data on number of droplets per bubble size and initial velocity size distribution were available. Moreover, the initial velocity is a challenging magnitude to calculate from experiments as the surface is highly agitated due to multiple bubble burst, and even complicated in churn turbulent flow regime where the droplets are generated by shear of water ligaments.

The equation developed by Andrews (1960) calculated the entrainment as a function of Boltzmann-Maxwell distribution of droplet velocities. However, Andrews's model does not give information on superficial gas velocity which is necessary to entrain droplets. Supposing that the superficial gas velocity is considered, the model is still limited as the Boltzmann-Maxwell function is applied to a steady-state conditions. Kruzhilin (1951) correlation considers only the gas kinetic energy. Yet, the information on height is not taken into account as the entrainment changes with height above the water surface. This latter was considered in the equation of Panasenko and Antonov (1959), nonetheless, the effect of pressure is missing in their model.

The height above the water pool, the gas kinetic energy, gas void fraction in the pool and effect of pressure was analyzed by Sterman et al. (1957), however, the operating pressure used was up to 185 bar, which affects greatly the hydrodynamics of the pool. It was reported that the bubble size decreases with increasing pressure.

Golub (1970) investigated the effect of height especially when the entrainment is dominated by deposition. The calculated entrainment decrease as the height increase for all gas velocities values. Golubs model is only applicable to deposition controlled region and high gas velocity.

Kataoka and Mamoru (1983) analysed the previous correlations and decided to decorticate the phenomena in detail. They subdivide the entrainment formulation as a function of height above the water pool as shown in Eqs. (17)–(19). The formulation of Kataoka and Ishii is of extreme precision in quantifying the entrainment comparing to previous correlations, nevertheless, their correlations are not applicable to low gas velocities (bubbly flow regime).

However, in large vessel diameter such as a containment building, the effect of deposition is neglected, and rather replaced by the effect of buoyancy (suspended droplets). For instance, in Kataoka and Ishii's model, the term $e^{-0.205\left(\frac{h}{D_H}\right)}$, which translate the droplet deposition onto vessel walls, does not contribute for large vessel diameter, where $D_H \to \infty$, implies $e^{-0.205\left(\frac{h}{D_H}\right)} \to 1$.

This effect is extensively investigated in THAI facility (Gupta et al., 2016) where experiments on re-entrainment of contaminants by water droplets are conducted in large vessels.

The developed correlations have a non-dimensional aspect, as dimensionless superficial gas velocity, dimensionless viscosity, dimensionless pool diameter and dimensionless height between the swell level and the top vessel. These numbers were obtained from analysing the entrainment phenomenon. Based on dimensional analysis, the superficial gas velocity is obtained by considering the kinetic energy of the streaming gas, the viscous force of the gas gives us the dimensionless viscosity. The dimensionless pool diameter is the Bond number. Cosandey (1999) added the effect of free convection to the aforementioned variables to develop the correlation in Eq. (20). This correlation is limited to low gas flow rates.

Furthermore, the geometry is one of the important factors affecting the entrainment if it is not the main one. For instance, during depressurization, in addition to the depressurization rate, the position of the vent is of extreme relevance to determining the hydrodynamics of the pool. Fig. 15 shows how the hydrodynamics are affected.

In Fig. 15 (right), the pool was depressurized from 1.5 MPa to atmospheric pressure, and the vent was at 2 *m* from the water surface. Under these conditions, the pool is highly agitated, and two flow regimes were observed according to Kudo et al. (1994), churn turbulent flow near the walls and heterogeneous bubbly flow away from the walls. That implies at least three mechanisms of droplet generation as shown in Fig. 2: bubble burst (bubbly flow regime), shear of ligament liquid (churn turbulent flow regime), and liquid impingement. Therefore, the entrainment of droplets would not be substantial. This is due to high turbulence intensity at the surface of the pool which enhances the collision between generated droplets (which more likely results in coalescence).

At THAI facility (Freitag and Schmidt, 2017), on the other hand, the vent was placed at 8 *m* from the water surface, and the pool was depressurized from 0.2888 MPa to 0.2376 in 1 h. As a result, only the surface was bubbling. Slow depressurization of the containment is to be expected during the late phase of severe accident in order to keep the containment integrity. Kudo et al. (1994) experiment shows the consequence of rapid depressurization. Indeed it re-entrains the previously deposited fission products from the pool, however, it causes churn turbulent flow which entrains less droplets. Causing churn turbulent flow regime in large pools might be one of the solutions to decrease the contribution of the source term.

It could be concluded that in large pool diameter, and in order to decrease the volatility of aerosols in the containment atmosphere, the pool must be strongly agitated.

Another factor that affects the entrainment is the Bernoulli's effect. This latter was notable in many experiments (Bagul et al., 2019), (Bagul et al., 2018a), (Bagul et al., 2018b) and (Kim and No, 2003), (Kim and No, 2005a, 2005b), (Sun et al., 2014), (Qiu et al., 2015), (Sun et al., 2015), (Xiang et al., 2016), and simulated numerically (Lu and Xie, 2017a), (Lu and Xie, 2017b), (Bagul et al., 2019), (Bagul et al., 2018b).

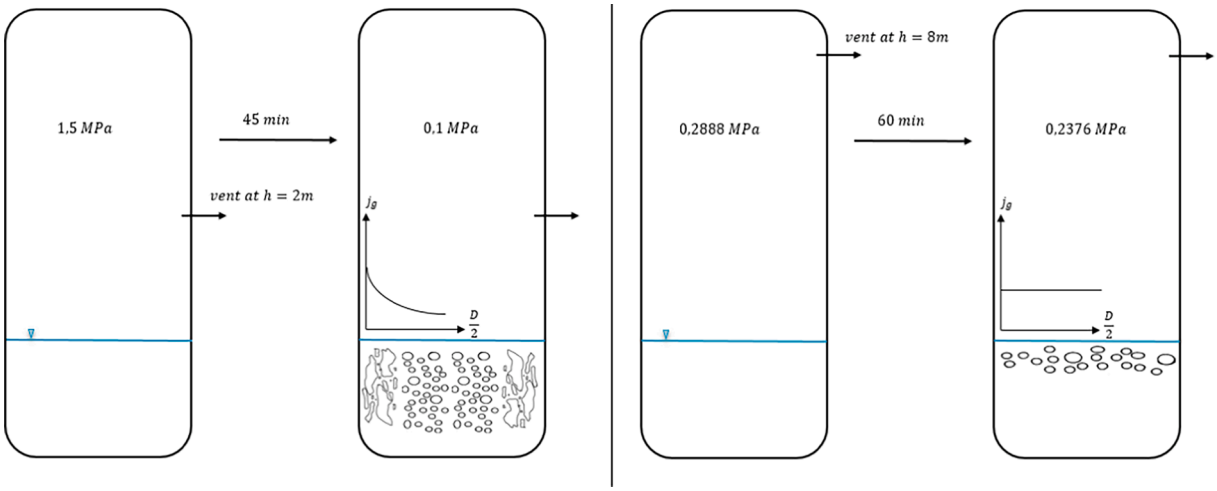

Fig. 15. Pool depressurization of Kudo experiment (Kudo et al., 1994) (right) and THAI experiments (Freitag and Schmidt, 2017)() (left).

Fig. 16 shows the Bernoulli effect for different scenarios, side exit, upward exit and the break that occurs during a SBLOCA scenario in a PWR. An important amount of entrainment could be measured from these scenarios due to the important momentum at each exit type. This effect was analysed by Kataoka and Mamoru (1983) and Rozen et al. (1976a). The variable that translates the Bernoulli effect in this case is the ratio of the dimensionless superficial gas velocity to dimensionless height above the pool $\left(\frac{j_g^*}{h^*}\right)^n$ power n corresponding to zone II and III (Table 4). The power n translate the acceleration of the gas passing the exit.

The diameter of the pool is the most important factor when analysing the entrainment phenomena as it defines the regime of two-phase flow. The carryover phenomena in pool are different from pipes. The two-phase flow regime in pipes are well defined due to the small domains (small diameter), so as the gas velocity increases we observe transition from one flow regime to another. Whereas the flow regime in a water pool (infinite diameter), the gas flowing as bubbles of different shapes moves chaotically, which characterizes the complexity of the two-phase flow in such cases. The Bond number in a pipe is much smaller than in a pool, which means, for an air–water system and at constant temperature, the gravitational force is more significant in a pool, which implies that more droplets will fall back to the water surface.

The maximum entrainment is 4 in Fig. 14 was measured from the experiment of Bagul et al. (2019). Kim and No (2003) measured a maximum entrainment 5.10^{-2} Fig. 17. Wallis (1962) measured a maximum entrainment of 20 (Fig. 18). In THAI experiments, the highest value of measured entrainment was 1.10^{-3} (Fig. 19**).** From these experiments, we can conclude that the entrainment decreases with increasing pool diameter and with an increase in the complexity of two-phase flow.

Table 8 shows the variation of water entrainment as a function of pool geometry. From these experiments, despite the pool diameter, the entrainment depend mainly on the height. It is shown that the entrainment decrease with increasing height above the water pool.

The potential energy in terms of pressure $\left(e_{pot} = \rho g h\right)$ is also an important factor. This could be translated to the height above the water surface$h$. The entrainment near the surface consists of all droplets as stated by Kataoka and Mamoru (1983) and decreases as h increases. The effect of pressure in the dimensionless height $h^* = h/\sqrt{\frac{g\Delta\rho}{\sigma}}$ was considered in most entrainment correlations, except the correlation of Kruzhilin (1951).

The Froude number in Cosandey's correlation (Cosandey, 1999), was considered as a droplet volatility condition. The rising droplets reached

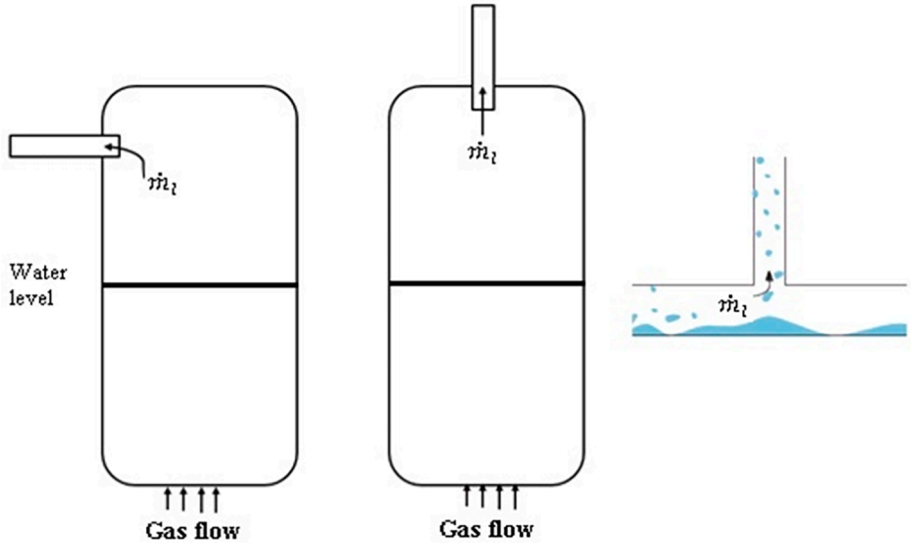

Fig. 16. Simulation of a SBLOCA scenario conducted by Lu and Xie (2017a) and Sun et al. (2014).

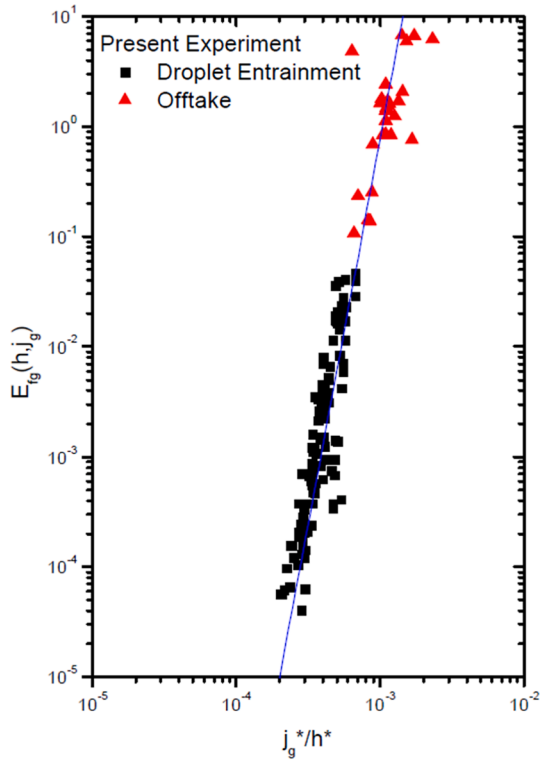

Fig. 17. Pool entrainment (TLOFW in PWR) Kim and No (2003).

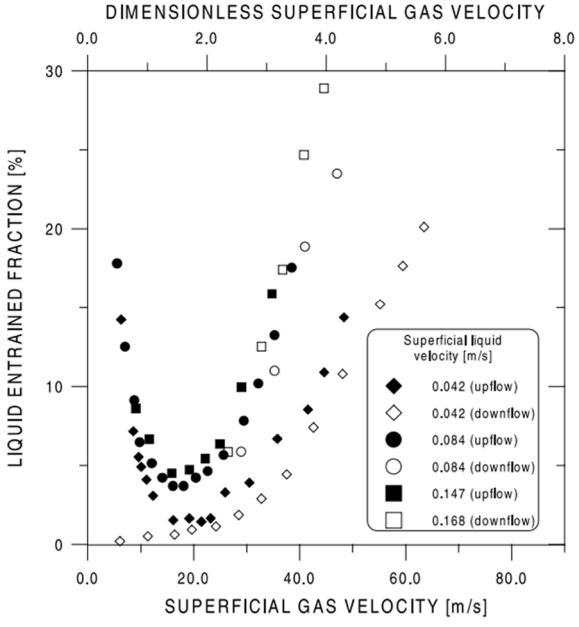

Fig. 18. Pipe entrainment Wallis (1962) (figure taken from (Barbosa et al., 2002)).

such height due to the kinetic energy of the gas. As swarm of the droplets rises, it interacts with the steaming gas by breaking into smaller droplets or droplet–droplet interaction, which lead to coalescence or breakup depending of the Weber number and the angle of the impact. The breakup mechanism is a function of height and gas velocity. If coalescence between groups of droplets of the same size occurs, the de-entrainment takes place again comparing gas velocity and droplet terminal velocity.

The droplets stability can be managed by analysing the Weber and Bond numbers. For $Bo \gg\gg 1$, and $We >>>1$ roughly, the droplet becomes unstable and breaks up.

This condition of the Bond and Weber numbers is kept until the droplet reached a critical size where the surface tension becomes more important. In this case, the droplet is assumed to be perfectly spherical and could be submitted to Stocke's flow regime.

The Rayleigh number *Ra*, in Cosandey's correlation, Eq. (20), is used to take into account the effect of turbulent diffusive transport of droplets from the pool surface to the overlaying atmosphere. The origin of this transport is the free convection caused by the temperature difference between the hot pool surface and the lower atmospheric temperature. It is superimposed by the advective transport caused by the gas flow from the pool surface upward. The Cosandey et al. paper suggests that during the experiment there are stationary equilibrium conditions in relation to entrainment and atmospheric droplet concentration conditions. How fast will this stationary state be established?

To a first approximation, neglecting the turbulent diffusive transport, the time to reach steady state is the travel time of droplets from the pool surface to the vessel outlet line (Cosandey, 1999) a distance of about $H = 2\ m$. When considering a full spectrum of droplet sizes, each size class travels upward with a different speed corresponding to the difference between the upward superficial gas velocity j_g and the downward size-dependent Stokes sinking velocity (or terminal velocity) v_t. The size class with sinking velocity equal to the superficial gas velocity is just suspended in the lower vessel region and will not be transported upward. Slightly smaller droplets will be carried upward at a very small velocity $u = j_g - v_t$, so it will take very long time $t_{eq} = H/u$ to reach atmospheric concentration equilibrium for this droplet size class. The smallest droplets will travel with almost the superficial velocity, so their time to reach equilibrium can be estimated by $t_{eq} = H/j_g$.

Even more complicated is the situation where turbulent diffusive transport is taken into account. This effect has the potential to generate a steady-state vertical droplet concentration profile in the atmosphere in the deposition-controlled region, which could be determined experimentally from the droplet size distribution. So far, this magnitude is not available in the open literature for large pool vessels.

An estimate for the droplet diffusion coefficient can be obtained by application of the heat and mass transfer analogy, starting with the Nusselt number for convective heat transfer above a horizontal surface instead of the Rayleigh number, and then, taking this as the Sherwood number for droplet concentration mass transfer. Droplets could be considered as traceable material (or tracer) in such estimate, following the turbulent motions without inertia.

Quantitative estimates of the time to reach equilibrium should be conducted for the actual experimental conditions; suitable Nusselt number correlations could be found in literature and textbooks. The establishment of a vertical droplet concentration profile in the deposition controlled region was not investigated by Cosandey et al., and the published data will probably not give information about this effect. The fact that Cosandey take into account the Rayleigh number in entrainment correlation at least indicates that convective turbulence is a relevant effect.

Pool water heat-up did probably not cause unsteady conditions because all experiments are conducted with boiling pool. Unsteady thermal conditions would have been quickly discovered by the thermocouples.

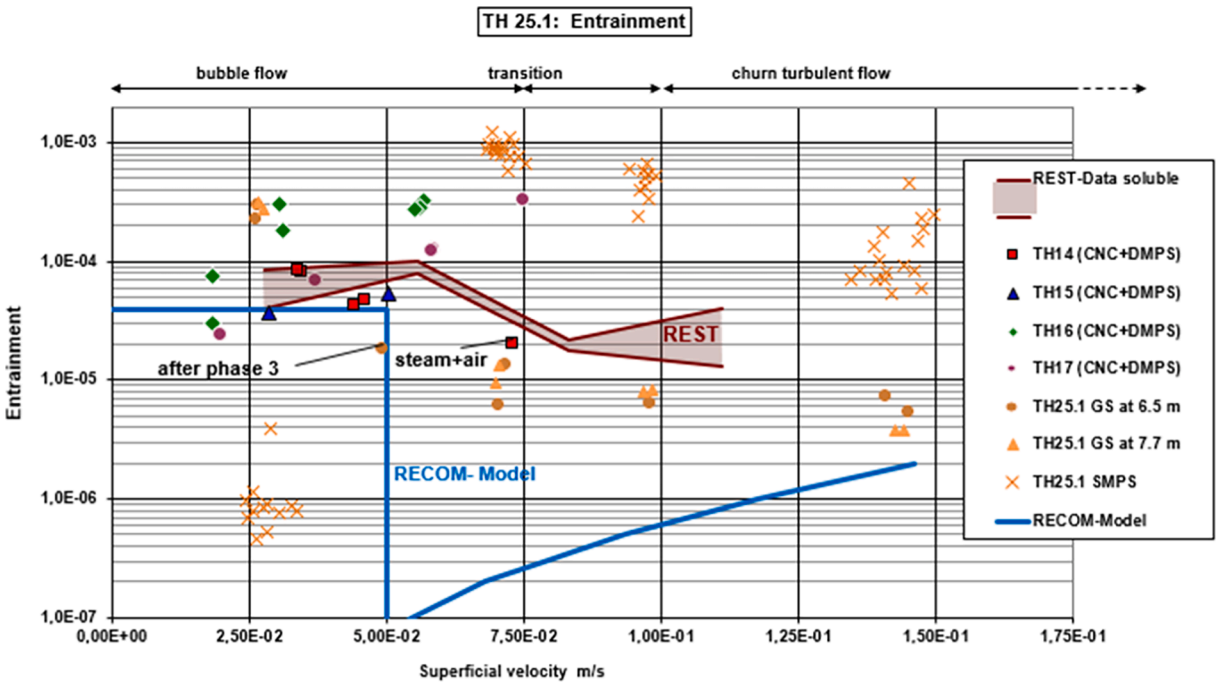

Fig. 19. Pool entrainment in THAI experiments (Schmidt et al., 2015).

Table 8
The effect of pool geometry on Entrainment.

	THAI (Schmidt et al., 2015)	Bagul et al. (2019)	Kim and No (2005a), Kim and No (2005b)	Walls (1962)
Pool diameter (m)	1.4	1.93	0.3	12.10^{-3}
Bond number	575.454	744.2	118.97	–
Height above water pool (m)	8	0.16	0.1 to 1	–
Sup. gas Vel. (m/s)	0.0287 to 0.0688	0.09 to 0.277	0.09 – 0.33	50
Entrainment	6.10^{-4}	0.371 – 4.900	0.01 - 0.1	20
Geometry	Large vessel	Small vessel	Small vessel	Pipe

6. Conclusion

This review provided experimental and analytical works on entrainment phenomena. It also provides the main shortcoming of the developed correlations by previous authors. It was identified that some correlation are either limited to a specific flow regime, or a specific zone above the water pool. Furthermore, explanations on discrepancies between some experimental data within the same superficial gas velocity range related to thermal-hydraulics and physical properties of the system was given.

Certainly, more variable needs to be investigated theoretically and experimentally, and this fact is related to the complexity of two-phase flows in pools. For instance, a variable that might need some attention is the concentration of droplets above the water pool at different locations. The concentration of the suspended droplets, which are more likely to be problematic in a containment building of nuclear power plant because it is hard to retain, is governed by the diffusion and advection/convection phenomena. It decreases as the gas velocity tends to infinity. The advection phenomenon is dominant over the diffusion, as the gas velocity increases, leading to the birth of large eddies.

CFD simulation showed efficiency on simulating the pool entrainment phenomena in the absence of suitable experimental data. However, CFD simulation require extensive computational resource especially in the micron and sub-micron range, where the mesh has to be fine to capture the droplets (mesh size 10 times smaller than the captured object).

Declaration of Competing Interest

The authors declare that they have no known competing financial interests or personal relationships that could have appeared to influence the work reported in this paper.

Acknowledgements

A special thanks to Dr. Pr. Karsten Fischer from Becker Technologies, Germany (retired) and Dr. Pr. Abdel Dehbi from Paul Scherrer Institute (PSI), Switzerland for their assistance and fruitful discussions which resulted in providing insights in the studied phenomena.

Funding

This research did not receive any specific grant from funding agencies in the public, commercial, or not-for-profit sectors.

References

Andrews, J.M., 1960. Kinetic study of fluidized solids entrainment. Ind. Engr. Chem. 52 (1), 85–88.
Arndt, S., Weber, G., Nowack, H., Spengler, C., Schwarz, S., Eschricht, D., Beck, S., 2015. COCOSYS User's Manual. Gesellschaft für Anlagen- und Reakt. mbH.
Azbel, D., 1981. Two Phase Flows in Chemical Engineering. Cambridge University Press.
Bagul, R.K., Pilkhwal, D.S., Limaye, S.P., Vijayan, P.K., Joshi, J.B., 2018a. Air Water Loop for investigation of flow dynamics in a steam drum: steady state two-phase natural circulation experiments and validation. Nucl. Eng. Des. 328, 266–282. https://doi.org/10.1016/j.nucengdes.2017.12.024.
Bagul, R.K., Pilkhwal, D.S., Vijayan, P.K., Joshi, J.B., 2018b. Air Water Loop for investigation of flow dynamics in a steam drum: carryover experiments and CFD simulation. Nucl. Eng. Des. 333, 145–160. https://doi.org/10.1016/j.nucengdes.2018.04.012.
Bagul, R.K., Pilkhwal, D.S., Vijayan, P.K., Joshi, J.B., 2019. Experimental investigations on carryover in a gravity separation-based steam drum. J. Nucl. Eng. Radiat. Sci. 5, 1–12. https://doi.org/10.1115/1.4041791.

Berzal, M.E., Crespo, M.J.M., Swiderska-Kowalczyk, M., Espigares, M.M., Jimenez, J.L., 1995. State-of-the-art review on fission products aerosol pool scrubbing under severe accident conditions. Eur. Comm. Brussels, Belgium.
Blanchard, D.C., 1989. The size and height to which jet drops are ejected from bursting bubbles in seawater. J. Geophys. Res. Ocean. 94 (C8), 10999. https://doi.org/10.1029/JC094iC08p10999.
Brenner, H., 2011. Phoresis in fluids. Phys. Rev. E - Stat. Nonlinear, Soft Matter Phys. 84 (6) https://doi.org/10.1103/PhysRevE.84.066317.
Clift, R., Grace, J.R., Weber, M.E., 1978. Bubbles, Drops, and Particles. Acad. Press.
Cosandey, J.O., von Rohr, P.R., 2001. Entrainment of soluble and non soluble tracers from a boiling water surface. Nucl. Eng. Des. 208 (1), 87–97. https://doi.org/10.1016/S0029-5493(01)00354-5.
Cosandey, J., 1999. Droplet production over a boiling pool during a slow depressurization. PhD thesis ETH Zürich, 179. DOI:10.3929/ethz-a-010782581.
Davis, R.F., 1940. The physical aspect of steam generation at high pressures and the problem of steam contamination. Proc. Inst, lech. Eng. 144 (1), 198–216.
de Santiago, M.R., Marvillet, C., 1991. Pool entrainment phenomenon: Measurement of size and velocity distributions of droplets at several distances above the bubbling surface. Int. Commun. Heat Mass Transf. 3, 499–511.
Dehbi, A., Guentay, S., Suckow, D., 1994. Design of the Test Matrix for P O S E I D O N Pool Scrubbing Experiments Using the B U S C A - P S I Code. J. Aerosol Sci. 25, 275–276.
Dehbi, A., Guentay, S., 1994. Simulation of Pool Scrubbing Experiments Using Busca. In: Third International Conference on Containment and Design, p. 16.
Dehbi, A., Suckow, D., Lind, T., Guentay, S., Danner, S., Mukin, R., 2016. Key findings from the artist project on aerosol retention in a dry steam generator. Nucl. Eng. Technol. 48 (4), 870–880. https://doi.org/10.1016/j.net.2016.06.001.
Freitag, M., Schmidt, E., 2017. Re-Entrainment of Fission Products from Water Pools at Elevated Temperature. Tech. Rep. No. 150 1516 – TR – WH24.
Fritz, B.G., 2006. Aerosol entrainment from a sparged non-newtonian slurry. J. Air Waste Manag. Assoc. 56 (8), 1108–1114. https://doi.org/10.1080/10473289.2006.10464531.
Gao, S., Fu, Y., Sun, D., Mei, Q., Pan, N., Zhang, S., Huang, G., 2017. Comparison research on different aerosol pool scrubbing models. Int. Conf. Nucl. Eng. Proc., ICONE 7, 1–7. https://doi.org/10.1115/ICONE25-66540.
Garner, F.H., Ellis, S.R.M., Lacey, J.A., 1954. The size distribution and entrainment of droplets. Trans. Inst. Chem. Eng. 32, 222–235.
Gephart, R.E., Lundgren, R.E., 1995. Hanford tank clean up: a guide to understanding the technical issues. Report. https://doi.org/10.2172/195769.
Golub, S.I., 1970. Investigation of moisture carryover and separation in evaporation apparatus, in: Candidates Dissertation. MEI.
Gupta, S., Herranz, L.E., Van Dorsselaere, J.., 2017. Integration of pool scrubbing research to Enhance Source Term calculations, in: Proceedings of the 8th European Review Meeting of Severe Accident Research (ERMSAR 2017),. Warsaw, Poland.
Gupta, S., Poss, G., Sonnenkalb, M., 2016. OECD / NEA THAI program for containment safety research: main insights and perspectives. EUrosafe Forum.
Kajimoto, M., Hidaka, A., Muramatsu, K., Sugimoto, J., 1988. A Computer Code for the Analysis of Radionuclide Transport and Deposition under Severe Accident Conditions: Model Description and User's Manual.
Kataoka, I., Mamoru, I., 1983. Mechanistic Modeling and Correlations for Pool Entrainment Phenomenon. Nureg/Cr-3304 ANL-83-37.
Kharoua, N., Khezzar, L., Saadawi, H., 2013. CFD modelling of a horizontal three-phase separator: a population balance approach. Am. J. Fluid Dyn. 3, 101–118. https://doi.org/10.5923/j.ajfd.20130304.03.
Kim, C.H., No, H.C., 2003. Liquid entrainment and off-take through the break at the top of a vessel. Trans. Am. Nucl. Soc. 89, 426.
Kim, Hyun C., No, Cheon H., 2005a. Liquid entrainment and off-take through the break at the top of a vessel. Nucl. Eng. Des. 235, 1675–1685. https://doi.org/10.1016/j.nucengdes.2005.01.014.
Kim, Chang Hyun, No, Hee Cheon, 2005b. Liquid entrainment and off-take through the break at the top of a vessel. Nucl. Eng. Des. 235 (16), 1675–1685. https://doi.org/10.1016/j.nucengdes.2005.01.014.
Koch, M.K., Voßnacke, A., Starflinger, J., Schütz, W., Unger, H., 2000. Radionuclide re-entrainment at bubbling water pool surfaces. J. Aerosol Sci. 31 (9), 1015–1028.
Kolokoltzev, V.A., 1952. An Investigation of the Conditions in the Steam Space of ISV Evaporators. Diss. Transl. Power Inst. 10.
Kruzhilin, G.N., 1951. The dependence of the permissible vapor load upon the pressure. Izv. Akad. Nauk. Otd. Tekh. Nauk. 7, 1106.
Kudo, T., Yamano, N., Moriyama, K., Maruyama, Y., Sugimoto, J., 1994. Experimental study of aerosol reentrainment experimental study of aerosol reentrainment from flashing pool in ALPHA program. In: The Third International Conference on Containment Design and Operation, p. 11.
Lhuissier, H., Villermaux, E., 2012. Bursting bubble aerosols. J. Fluid Mech. 696, 5–44. https://doi.org/10.1017/jfm.2011.418.
Lu, M., Xie, H., 2017b. A Numerical Study of Liquid Carryover Based on The Volume of Fluid Model. ICONE25-66292.
Lu, M., Xie, H., 2017a. An investigation of pool entrainment based on the method of Volume of Fluid. Nucl. Eng. Des. 318, 72–84. https://doi.org/10.1016/j.nucengdes.2017.04.006.
Moody, F.J., Nagy, S.G., 1983. Estimated effects of interfacial vaporization on fission product scrubbing. ANS-ENS Int. Meet. Light Water React. Sev. Accid. Eval. 11.5.1-11.5–8.
Norman, T.L., Revankar, S.T., Ishii, M., 2006. Steam-air mixture condensation in a subcooled water pool.
Owczarski, P.C., Burk, K.W., 1991. SPARC-90: A Code for Calculating Fission Product Capture in Suppression Pools. Nucl. Regul. Comm. Washington, DC (United States). Div. Regul. Appl. NUREG/CR-5765; PNL-7723 ON: TI92003256.
Özdemir, S., 2005. Investigation of Air Bubble Motion in Water Through a Vertical Narrow Rectangular Channel by Using Image Processing Techniques. PhD thesis, METU -. Middle East Tech. Univ.
Panasenko, M.D., Antonov, A.I., 1959. Correlation of mechanical carryover by steam. Teploenergetika 6.
Paradissiadis, von I., Widmer, F., 1984. Prediction of liquid entrainment in evaporators. Chem. Eng. Process. Process Intensif. 18 (5), 249–253.
Parozzi, F., Paci, S., 2006. Development and validation of the ECART code for the safety analysis of nuclear installations. Int. Conf. Nucl. Eng. Proceedings, ICONE 2006. DOI:10.1115/ICONE14-89275.
Poulain, S., Villermaux, E., Bourouiba, L., 2018. Ageing and burst of surface bubbles. J. Fluid Mech. 851, 636–671. https://doi.org/10.1017/jfm.2018.471.
Qiu, S.Z., Sun, D.C., Tian, W.X., Xiang, Y., Su, G.H., 2015. Experimental and Theoretical Research on Liquid Entrainment in AP1000 ADS Blow - down Phase of SBLOCA. NURETH-16.
Ramsdale, S.A., Bamford, G.J., Fishwick, S., Starkie, H.C., 1992. Status of research and modelling of water-pool scrubbing EUR 14566 EN.
Ramsdale, S.A., 1995. Busca-Jun91 Reference Manual.
Rozen, A.M., Golub, S.I., Davydov, I.F., Gostinin, G.I., 1970. Some Laws Governing Drop Carry Over, in: Soviet Physics Doklady. p. 648.
Rozen, A.M., Golub, S.I., Votintseva, T.I., 1976a. Calculating droplet carryover with bubbling. Teploenergetika 23, 59.
Rozen, A.M., Golub, S.I., Votintseva, T.I., 1976b. On the nature of degree of dependence of transported carryover on vapor velocity with bubbling. Teploenergetika 23, 55.
Schmidt, E.W., Gupta, S., Freitag, M., Poss, G., Laufenberg, B. Von, 2015. Wet Resuspension of Insoluble Material from a Boiling Sump. ICONE23-2060.
Schmitz, B.M., 2000. Pool Scrubbing Module SPARC-B/98 for SOPHAEROS V2mod0_1 - Model Description - 1, 220.
Shah, Y.T., Kelkar, B.G., Godbole, S.P., Deckwer, W.-D., 1982. Design parameters estimations for bubble column reactors. AIChE J. 28 (3), 353–379. https://doi.org/10.1002/(ISSN)1547-590510.1002/aic.v28:310.1002/aic.690280302.
Spiel, Donald E., 1998a. On the births of film drops from bubbles bursting on seawater surfaces smaller than their parents and which have upward velocity oscillation. J. Geophys. Res. 103 (C11), 24907–24918.
Spiel, Donald E., 1998b. On the births of film drops from bubbles bursting on seawater surfaces. J. Geophys. Res. Ocean. 103 (C11), 24907–24918. https://doi.org/10.1029/98JC02233.
Sterman, L.S., 1957. The correlation of experimental data for vapour bubbling through a liquid. Zh. Tekh. Fiz. 26, 1519.
Sterman, L.S., 1958. On the theory of steam separation. Sov. Phys.-Technical Phys. 3, 1440–1451.
Sterman, L.S., Antonov, A.I., Surnov, A.V., 1957. An investigation of steam quatility at 185 atm. Teploenergetika 3, 17.
Sterman, L.S., Antonov, A.I., Surnov, A. V, 1958. An Investigation of the Steam Quality at 185 atm Using Radioactive Isotopes. Teploteh. i Gidrodynamika.
Sterman, L.S., 1952. Kotloturbostroenie. no. 5.
Styrikovich, M.A., Sterman, L.S., Surnov, A.V., 1955. An investigation of the carry over of salt by steam using radioactive isotopes. Teploenergetika 2.
Styrikovich, M.A., Petukhov, V.I., Kolokoltsev, V.A., 1964. The effect of gas phases density on the extent of droplet entrainment. Teploenergetika 11.
Sun, D.C., Tian, W.X., Qiu, S.Z., Su, G.H., Zhang, P., Liu, J.C., Ma, Y.Y., 2014. Scaling analysis of AP1000 ADS-4 entrainment and depressurization. Prog. Nucl. Energy 74, 71–78. https://doi.org/10.1016/j.pnucene.2014.01.019.
Sun, D.C., Xiang, Y., Tian, W.X., Liu, J.C., Zhang, P., Qiu, S.Z., Su, G.H., 2015. Experimental investigation of upper plenum entrainment in AP1000. Prog. Nucl. Energy 80, 80–85. https://doi.org/10.1016/j.pnucene.2014.12.003.
TOBA, Yoshiaki, 1959. Drop production by bursting of air bubbles on the sea surface (II) theoretical study on the shape of floating bubbles. J. Oceanogr. Soc. Japan 15 (3), 121–130. https://doi.org/10.5928/kaiyou1942.15.121.
Viles, J.C., 1993. Predicting liquid re-entrainment in horizontal separators. JPT. J. Pet. Technol. 45, 405–409. https://doi.org/10.2118/25474-PA.
Wallis, G.B., 1962. The Onset of Droplet Entrainment in Annular Gas-Liquid Flow. Schenectady, NY.
Wassel, A.T., Mills, A.F., Bugby, D.C., Oehlberg, R.N., 1985. Analysis of radionuclide retention in water pools. Nucl. Eng. Des. 90 (1), 87–104. https://doi.org/10.1016/0029-5493(85)90033-0.
Westgarth, R., 1964. Chamber geometry in multi-stage flash evaporators. U.S. Dep. Commer. Off. Tech. Serv.
Wurster, S., Meyer, J., Kolb, H.E., Kasper, G., 2015. Bubbling vs. blow-off - on the relevant mechanism(s) of drop entrainment from oil mist filter media. Sep. Purif. Technol. 152, 70–79. https://doi.org/10.1016/j.seppur.2015.08.012.
Xiang, Y., Wu, Y.W., Sun, D.C., Tian, W.X., Zhang, P., Qiu, S.Z., Su, G.H., 2016. Experimental simulation of liquid entrainment in ADS-4 depressurization line in AP1000. Prog. Nucl. Energy 91, 295–301. https://doi.org/10.1016/j.pnucene.2016.05.006.
Yeh, G., Zuber, N., 1960. On the proplem of liquid entrainment. Report.
Zenz, F.A., Weil, N.A., 1958. A theoretical-empirical approach to the mechanism of particle entrainment from fluidized beds. AIChE J. 4 (4), 472–479. https://doi.org/10.1002/(ISSN)1547-590510.1002/aic.v4:410.1002/aic.690040417.
Zhang, Jiaqi, Chen, John J.J., Zhou, Naijun, 2012. Characteristics of jet droplet produced by bubble bursting on the free liquid surface. Chem. Eng. Sci. 68 (1), 151–156. https://doi.org/10.1016/j.ces.2011.09.019.